J Elast
DOI 10.1007/s10659-012-9372-7

# On Pressurized Curvilinearly Orthotropic Circular Disk, Cylinder and Sphere Made of Radially Nonuniform Material

**Vlado A. Lubarda**

Received: 25 September 2011


**Abstract** A unified analysis is presented for the elastic response of a pressurized cylindrically anisotropic hollow disk under assumed conditions of plane stress, or a hollow cylinder under plane strain conditions, and a spherically anisotropic hollow sphere, made of material which is nonuniform in the radial direction according to the power law relationship. The solution for a cylinder under generalized plane strain is also presented. Two parameters play a prominent role in the analysis: the material nonuniformity parameter $m$, and the parameter $\varphi$ which accounts for the combined effects of material anisotropy, represented by the specified parameters $(\alpha, \beta, \gamma)$, and material nonuniformity, represented by the parameter $m$. The radial and circumferential stresses are the linear combinations of two power functions of the radial coordinate, whose exponents ($n_1$ and $n_2$) depend on the parameters $m$ and $\varphi$. New light is added to the stress amplification and shielding under combined effects of curvilinear anisotropy and radial nonuniformity. Different loading combinations are considered, including the equal pressure at both boundaries, and the uniform pressure at the inner or the outer boundary. While the stress state for the equal pressure loading is uniform in the case of isotropic uniform material ($m = 0$, $\varphi = 1$), and for one particular radially nonuniform and anisotropic material, it is strongly nonuniform for a general anisotropic or nonuniform material. If the aspect ratio of the inner and outer radii decreases (small hole in a large disk/cylinder or sphere), the magnitude of the circumferential stress at the inner radius increases for $n_1 > 0$ (stress amplification), and decreases for $n_1 < 0$ (stress shielding). Both can be achieved by various combinations of the material parameters $m$, $\alpha$, $\beta$, and $\gamma$. While the stress amplification in the case of a pressurized external boundary occurs readily, it occurs only exceptionally in the case of a pressurized internal boundary. The effects of material parameters on the displacement response are also analyzed. The approximate character of the plane stress solution of a pressurized thin disk is discussed and the results are compared with those obtained by numerical solution of the exact three-dimensional disk model.

V.A. Lubarda (✉)
Department of Mechanical and Aerospace Engineering, University of California, San Diego, La Jolla, CA 92093-0411, USA
e-mail: vlubarda@ucsd.edu

V.A. Lubarda
Montenegrin Academy of Sciences and Arts, Rista Stijovića 5, 81000 Podgorica, Montenegro

Published online: 29 February 2012

**Keywords** Curvilinear anisotropy · Lamé problem · Radial nonuniformity · Stress amplification · Stress shielding

**Mathematics Subject Classification (2000)** 74B05 · 74E05 · 74E10

## 1 Introduction

The effects of curvilinear anisotropy or radial nonuniformity of the material on the stress response in thick-walled disks, cylinders and spheres under different loading conditions have been studied extensively over number of years [3–13, 16–22, 25–27, 30–32]. Some remarkable features of the stress and displacement response, absent in the case of elastic isotropy and uniformity, but present in the case of even a slightest curvilinear anisotropy or radial nonuniformity, have been observed and discussed. Specifically, the stress amplification caused by focusing of a curvilinear anisotropy, or by a strongly enhanced material stiffness around a small hole in a nonuniform plate, as well as the stress shielding effects arising for certain values of the material parameters, have been examined in detail. These studies are of technological interest for manufacturing of fiber composites, processing of the functionally graded materials (FGM), casting of metals, wood industry (tree trunks), etc. For example, the microstructure of functionally graded materials is spatially varied (tailored) on a macroscale to improve their oxidation properties, and wear and thermal resistance [8]. In a composite metal-ceramic layered material, a FGM is inserted as an interface layer to reduce thermal stresses, improve bonding strength, and prevent delamination [14]. FGM coatings are superior to conventional ceramic coatings, showing significantly less damage under thermal shocks; see [19] and the references therein.

The objective of this paper is to present a unified analysis of the elastic response of a pressurized cylindrically anisotropic (locally orthotropic) hollow thin disk under plane stress approximation (the terminology "cylindrically orthotropic" is also often used [7]), or a hollow cylinder under plane strain conditions, and a spherically anisotropic (locally transversely isotropic) hollow sphere, all made of material which is nonuniform in the radial direction according to the power law relationship. The solution for a cylinder under generalized plane strain is also presented. Two parameters play a prominent role in the analysis: the material nonuniformity parameter $m$, and the parameter $\varphi$ which accounts for the combined effects of material anisotropy, represented by the specified parameters $(\alpha, \beta, \gamma)$, and nonuniformity of the elastic moduli, represented by the parameter $m$. The coefficients of lateral contraction are assumed to be independent of the position. The radial and circumferential stresses are the linear combinations of two power functions of the radial coordinate, whose exponents ($n_1$ and $n_2$) depend on the parameters $m$ and $\varphi$. The analysis sheds new light to the stress amplification and shielding under the combined effects of curvilinear anisotropy and radial nonuniformity of the material. Different loading combinations are examined, such as the equal pressure at both boundaries, or the uniform pressure at the inner or the outer boundary. While the stress state for the equal pressure loading is uniform in the case of isotropic uniform material ($m = 0$, $\varphi = 1$), and for one particular radially nonuniform anisotropic material, it is strongly nonuniform for a general anisotropic or nonuniform material. If the aspect ratio of the inner and outer radii decreases (small hole in a large disk/cylinder or sphere), the magnitude of the circumferential stress at the inner radius increases for $n_1 > 0$ (stress amplification), and decreases for $n_1 < 0$ (stress shielding). Both can be achieved by various combinations of the material parameters $m, \alpha, \beta$, and $\gamma$. For example, if the material is uniform ($m = 0$), the condition $n_1 < 0$ implies that $\varphi > 1$, i.e., $(\alpha - \gamma) > (j - 1)\beta$, where

$j = 1$ for a disk or cylinder, and $j = 2$ for a sphere. While the stress amplification in the case of a pressurized external boundary occurs readily, it occurs only exceptionally in the case of a pressurized internal boundary. The effects of material parameters on the displacement response are also analyzed. The approximate character of the plane stress solution of a pressurized thin disk is discussed and the results are compared with those obtained by numerical solution of the full three-dimensional disk model. It is shown that for a mildly nonuniform and isotropic thin disk the plane stress model yields accurate values for the radial and circumferential stress components, although it does not account for small values of out-of-plane stress components present in the three-dimensional disk model. The solution for other three types of boundary conditions, which correspond to prescribed displacements at both boundaries, prescribed traction at one boundary and displacement at another, and vice versa, will be reported elsewhere [24].

## 2 Cylindrical and Spherical Anisotropies

We consider a cylindrically anisotropic thin disk under the assumed conditions of plane stress, or long cylinder under the plane strain conditions, made of the material which is locally orthotropic, with the principal axes of orthotropy in the $(r, \theta, z)$ directions, and a spherically anisotropic sphere made of the material which is at any point transversely isotropic around the radial direction. The corresponding stress-strain relations, in the range of infinitesimally small elastic deformations, are

$$\epsilon_r = \frac{1}{E_\theta}(\alpha\sigma_r - j\beta\sigma_\theta), \qquad \epsilon_\theta = \frac{1}{E_\theta}(\gamma\sigma_\theta - \beta\sigma_r), \tag{2.1}$$

where

$$j = \begin{cases} 1, & \text{for a disk and cylinder,} \\ 2, & \text{for a sphere.} \end{cases} \tag{2.2}$$

The material parameters $(\alpha, \beta, \gamma)$ are defined by

$$\alpha = \begin{cases} k, \\ k(1 - \nu_{rz}\nu_{zr}), \\ k, \end{cases} \qquad \beta = \begin{cases} \nu_{\theta r}, \\ \nu_{\theta r} + \nu_{\theta z}\nu_{zr}, \\ \nu_{\theta r}, \end{cases} \qquad \gamma = \begin{cases} 1, & \text{for a disk,} \\ 1 - \nu_{z\theta}\nu_{\theta z}, & \text{for a cylinder,} \\ 1 - \nu_{\phi\theta}, & \text{for a sphere.} \end{cases} \tag{2.3}$$

The coefficient

$$k = \frac{E_\theta}{E_r} > 0 \tag{2.4}$$

specifies the degree of anisotropy. If $k < 1$, the material is stiffer in the radial direction than in the circumferential direction, the opposite being true for $k > 1$. The coefficient of lateral contraction $\nu_{\theta r}$ stands for the coefficient of lateral contraction in the $r$-direction due to stress in the $\theta$-direction, and likewise for other coefficients of lateral contraction. In the case of cylindrical anisotropy, the coefficients of lateral contraction are related by the symmetry relations

$$E_r\nu_{\theta r} = E_\theta\nu_{r\theta}, \qquad E_\theta\nu_{z\theta} = E_z\nu_{\theta z}, \qquad E_z\nu_{rz} = E_r\nu_{zr}, \tag{2.5}$$

so that the ratios of elastic moduli can be expressed as

$$k=\frac{E_\theta}{E_r}=\frac{\nu_{\theta r}}{\nu_{r\theta}}=\frac{\nu_{\theta z}\nu_{zr}}{\nu_{z\theta}\nu_{rz}},\qquad \frac{E_\theta}{E_z}=\frac{\nu_{\theta z}}{\nu_{z\theta}}=\frac{\nu_{\theta r}\nu_{rz}}{\nu_{r\theta}\nu_{zr}}. \tag{2.6}$$

Furthermore, by the positive-definiteness of the strain energy function, the elastic moduli are positive and the coefficients of lateral contraction are constrained by

$$\begin{cases} 0<\nu_{r\theta}\nu_{\theta r}<1, \qquad 0<\nu_{\theta z}\nu_{z\theta}<1, \qquad 0<\nu_{zr}\nu_{rz}<1,\\ \nu_{r\theta}\nu_{\theta r}+\nu_{\theta z}\nu_{z\theta}+\nu_{zr}\nu_{rz}+\nu_{rz}\nu_{z\theta}\nu_{\theta r}+\nu_{zr}\nu_{\theta z}\nu_{r\theta}<1. \end{cases} \tag{2.7}$$

In view of (2.6), the constraint $0<\nu_{r\theta}\nu_{\theta r}<1$ sets the bounds on $\nu_{\theta r}$ and $\nu_{r\theta}$ to be

$$-k^{1/2}<\nu_{\theta r}<k^{1/2}, \qquad -k^{-1/2}<\nu_{r\theta}<k^{-1/2}, \tag{2.8}$$

both coefficients being simultaneously either positive or negative. Since $k>0$ can in principle be any positive number, the coefficients $\nu_{\theta r}$ and $\nu_{r\theta}$ could be either greater or smaller than 1, albeit their product must be positive and less than 1. In view of (2.6), it is also noted that $\nu_{zr}\nu_{\theta z}\nu_{r\theta}=\nu_{rz}\nu_{z\theta}\nu_{\theta r}$. For the elaboration on the bounds on the coefficients of lateral contraction for orthotropic and transversely isotropic materials, see [28, 33]. In particular, Poisson's ratio for anisotropic materials can have no bounds [33].

In the case of spherical anisotropy considered in this work ($E_\phi=E_\theta$, $\nu_{\theta\phi}=\nu_{\phi\theta}$, $\nu_{r\theta}=\nu_{r\phi}$, $\nu_{\theta r}=\nu_{\phi r}$), the conditions (2.7) reduce to

$$-1<\nu_{\phi\theta}<1, \qquad \nu_{r\theta}\nu_{\theta r}<1, \qquad \nu_{\phi\theta}+2\nu_{r\theta}\nu_{\theta r}<1, \tag{2.9}$$

with the bounds on $\nu_{\theta r}$ and $\nu_{r\theta}$ as in (2.8).

If $E_\theta>E_r$ (i.e., $k>1$), the cylindrical anisotropy is referred to as the circumferentially orthotropic; if $E_r>E_\theta$ (i.e., $k<1$), it is referred to as the radially orthotropic [13, 16]. If the material is isotropic, $k=1$ and the parameters $\alpha$, $\beta$, and $\gamma$ in (2.3) reduce to

$$\alpha=\begin{cases}1,\\ 1-\nu^2,\\ 1,\end{cases} \qquad \beta=\begin{cases}\nu,\\ \nu(1+\nu),\\ \nu,\end{cases} \qquad \gamma=\begin{cases}1, & \text{for a disk,}\\ 1-\nu^2, & \text{for a cylinder,}\\ 1-\nu, & \text{for a sphere,}\end{cases} \tag{2.10}$$

becoming only $\nu$-dependent. In particular, $\alpha+\beta=1+\nu$ in all three cases, while $\beta/\gamma$ equals $\nu$ for a disk, and $\nu/(1-\nu)$ for a cylinder or a sphere.

## 3 Radial Nonuniformity

In addition to the described anisotropy properties, it will be assumed that a disk, cylinder or sphere are made of the material which is nonuniform in the radial direction, such that its elastic moduli vary in the radial direction according to the power-law relations

$$E_r=E_r^b\left(\frac{r}{b}\right)^m, \qquad E_\theta=E_\theta^b\left(\frac{r}{b}\right)^m, \qquad E_z=E_z^b\left(\frac{r}{b}\right)^m. \tag{3.1}$$

The exponent $m$ is a real number, reflecting the degree of nonuniformity of the material, and $(E_r^b, E_\theta^b, E_z^b)$ are the elastic moduli at the outer boundary $r=b$. If $m>0$, the elastic stiffness increases outward, from $r=a$ to $r=b$. The opposite is true for $m<0$. If $m=0$,

the material is uniform. The radial moduli at two boundaries are related by $E_r^a = c^m E_r^b$, where $c = a/b$ is the aspect ratio, with the similar relations for the elastic moduli in other two directions ($E_\theta$ and $E_z$). The same $m$ is used for all three moduli, so that the ratios of the moduli in different directions are constant, e.g., $E_\theta/E_r = E_\theta^b/E_r^b = k = \text{const}$. For latter use, it is also noted that the rate of the radial elastic modulus is $\mathrm{d}E_r/\mathrm{d}r = (m/r)E_r$, and similarly for other moduli.

The material nonuniformity of power-law type (3.1) has been previously used in [11, 17, 22]. Other types of nonuniformity can be considered, if needed to better match a specific functional grading of material. For example, the elastic moduli which vary exponentially with the square of the radial coordinate were adopted in [25, 34]. The adoption of the power-law spatial dependence (3.1) greatly affects the stress and deformation response through the sign and the magnitude of the exponent $m$. Generally speaking, for $m > 0$ there is a tendency for stress shielding, and for $m < 0$ for stress amplification. In a solid disk or sphere with $m > 0$, (3.1) predicts that the elastic modulus vanishes at the center, which may result in the displacement singularity at that point [11].

All coefficients of lateral contraction are assumed to be independent of $r$, which considerably simplifies the mathematical aspects of the analysis and is in accord with an assumption commonly used in the mechanics of functionally graded materials [8, 19], where it is known that the spatial variation of the Poisson ratio is of much less practical significance than that of the elastic moduli [17]. The spatial variation of both the elastic modulus and Poisson's ratio was considered in [12].

If the material is functionally graded so that the moduli ratios at $r = a$ and $r = b$ are equal to a prescribed value, say $\rho$, i.e.,

$$\frac{E_r^a}{E_r^b} = \frac{E_\theta^a}{E_\theta^b} = \frac{E_z^a}{E_z^b} = \rho, \tag{3.2}$$

then the exponent $m$ in (3.1) must be

$$m = \frac{\ln \rho}{\ln c}, \quad c = \frac{a}{b}. \tag{3.3}$$

In order that the strain energy density is positive-definite, the elastic moduli (3.1) have to be positive at any point. Thus, if $m > 0$, the outer radius $b$ in the considered model must be finite, for otherwise the elastic moduli would vanish at any internal point $r < b$. The outer radius must also be finite in order that the elastic moduli (3.1) are finite for $m < 0$.

## 4 Governing Differential Equations

The uniform pressure loading at two boundaries is considered, which implies that the circumferential component of displacement is zero. It will also be assumed that the radial component of displacement depends on the radial distance only, $u = u(r)$. This assumption is exact for the long cylinders under plane strain or generalized plane strain, as well as for the pressurized sphere, but is only an approximation in the case of a radially nonuniform cylindrically anisotropic disk (Appendix A). Correspondingly, the stress components $\sigma_r$ are $\sigma_\theta$ are also taken to be $r$-dependent only. In the absence of body force, the equilibrium equation is

$$\frac{\mathrm{d}\sigma_r}{\mathrm{d}r} + j\frac{\sigma_r - \sigma_\theta}{r} = 0, \tag{4.1}$$

where $j$ is given by (2.2). The strain-displacement relations are

$$\epsilon_r = \frac{\mathrm{d}u}{\mathrm{d}r}, \qquad \epsilon_\theta = \frac{u}{r}, \tag{4.2}$$

with the corresponding Saint-Venant compatibility condition

$$\frac{\mathrm{d}\epsilon_\theta}{\mathrm{d}r} + \frac{\epsilon_\theta - \epsilon_r}{r} = 0. \tag{4.3}$$

It is noted from (4.1) and (4.3) that $\sigma_r$ is an extremum when $\sigma_r = \sigma_\theta$ [30], while $\epsilon_\theta$ is an extremum when $\epsilon_r = \epsilon_\theta$.

By substituting the stress-strain relations (2.1) into (4.3), and by using the equilibrium equation (4.1) to eliminate $\mathrm{d}\sigma_r/\mathrm{d}r$, we obtain the Beltrami–Michell compatibility condition [23]

$$\frac{\mathrm{d}\sigma_\theta}{\mathrm{d}r} + \frac{1}{r}\big[(1-m)\sigma_\theta - \varphi\sigma_r\big] = 0, \tag{4.4}$$

where

$$\varphi = \frac{1}{\gamma}\big[\alpha + \beta(1-j)\big] - m\,\frac{\beta}{\gamma}. \tag{4.5}$$

The parameter $\varphi$ accounts for the combined effects of the state of anisotropy, represented by the parameters $\alpha$, $\beta$ and $\gamma$, and the degree of nonuniformity, represented by the parameter $m$. Specifically,

$$\varphi = \begin{cases} k - m\nu_{\theta r}, & \text{for a disk,} \\ \frac{k(1-\nu_{rz}\nu_{zr}) - m(\nu_{\theta r} + \nu_{\theta z}\nu_{zr})}{1-\nu_{\theta z}\nu_{z\theta}}, & \text{for a cylinder,} \\ \frac{k-(1+m)\nu_{\theta r}}{1-\nu_{\phi\theta}}, & \text{for a sphere.} \end{cases} \tag{4.6}$$

Upon differentiating (4.1) and incorporating (4.4), it follows that the radial stress is governed by the differential equation

$$r^2\frac{\mathrm{d}^2\sigma_r}{\mathrm{d}r^2} + (2 + j - m)r\frac{\mathrm{d}\sigma_r}{\mathrm{d}r} + j(1 - m - \varphi)\sigma_r = 0. \tag{4.7}$$

### 4.1 Radial Dependence of the Spherical Part of Stress

It is instructive to examine the radial dependence of the spherical part of stress tensor $(\sigma_r + j\sigma_\theta)/3$. To that goal, and with the help of (4.1), equation (4.4) can be rewritten as

$$\frac{\mathrm{d}}{\mathrm{d}r}\big[(1-m)\sigma_r + j\sigma_\theta\big] + j(1 - m - \varphi)\frac{\sigma_r}{r} = 0. \tag{4.8}$$

If the material is uniform ($m = 0$), this reduces to

$$\frac{\mathrm{d}}{\mathrm{d}r}(\sigma_r + j\sigma_\theta) + j(1-\varphi)\frac{\sigma_r}{r} = 0. \tag{4.9}$$

If the material is both uniform and isotropic, $\varphi = 1$ and

$$\frac{\mathrm{d}}{\mathrm{d}r}(\sigma_r + j\sigma_\theta) = 0, \tag{4.10}$$

confirming the well-known results that $\sigma_r+\sigma_\theta=$ const. for a disk or cylinder, and $\sigma_r+2\sigma_\theta=$ const. for a sphere [29]. On the other hand, if the material is anisotropic or nonuniform, the sum $(\sigma_r+j\sigma_\theta)$ is not constant, but $r$-dependent. Indeed, from (4.8),

$$\sigma_r+j\sigma_\theta=m\sigma_r-j(1-m-\varphi)\int\frac{\sigma_r}{r}\,\mathrm{d}r. \tag{4.11}$$

## 5 Stress and Displacement Expressions

The general solution of the second-order differential equation (4.7) is

$$\sigma_r=Ar^{-n_1}+Br^{-n_2}, \tag{5.1}$$

where $A$ and $B$ are integration constants and

$$n_{1,2}=\frac{1}{2}(1+j-m\mp s),\quad s=\left[(1+j-m)^2-4j(1-\varphi-m)\right]^{1/2}, \tag{5.2}$$

with $n_2-n_1=s$.

In order that $s$ is positive real number, the condition must hold $(1+j-m)^2>4j(1-\varphi-m)$, i.e., $m^2+4\varphi>0$ for a disk or cylinder, and $(1+m)^2+8\varphi>0$ for a sphere. Since $\varphi$ is defined by (4.6), these conditions are

$$\begin{cases} m^2-4m\nu_{\theta r}+4k>0, & \text{for a disk,}\\ m^2(1-\nu_{\theta z}\nu_{z\theta})-4m(\nu_{\theta r}+\nu_{\theta z}\nu_{zr})+4k(1-\nu_{rz}\nu_{zr})>0, & \text{for a cylinder,}\\ (1+m)^2(1-\nu_{\phi\theta})-8(1+m)\nu_{\theta r}+8k>0, & \text{for a sphere.}\end{cases} \tag{5.3}$$

By using the constraints (2.7)–(2.9), imposed on the coefficients of lateral contraction by the positive-definiteness of the strain energy, it can be verified (Appendix C) that the conditions (5.3) are always satisfied.

The exponents $n_1$ and $n_2$ in (5.1) account for the effects of the material nonuniformity and elastic anisotropy, represented by the parameters $m$ and $\varphi$, on the stress response. If the material is isotropic and uniform ($m=0$, $\varphi=1$), then $s=1+j$, $n_1=0$, and $n_2=1+j$.

If the material is isotropic but nonuniform ($m\neq0$), then $\varphi=1-(\beta/\gamma)m$, where $(\beta/\gamma)=\nu$ for a disk, and $(\beta/\gamma)=\nu/(1-\nu)$ for a cylinder or a sphere. In this case $s=[(1+j-m)^2+4jm(1-\beta/\gamma)]^{1/2}$, so that

$$n_{1,2}=\begin{cases}\frac{1}{2}(2-m\mp s), & s=(4-4\nu m+m^2)^{1/2}, & \text{for a disk,}\\ \frac{1}{2}(2-m\mp s), & s=(4-\frac{4\nu m}{1-\nu}+m^2)^{1/2}, & \text{for a cylinder,}\\ \frac{1}{2}(3-m\mp s), & s=[(3-m)^2+8m\frac{1-2\nu}{1-\nu}]^{1/2}, & \text{for a sphere.}\end{cases} \tag{5.4}$$

If the material is uniform ($m=0$) but anisotropic, then

$$s=\begin{cases}2\varphi^{1/2}, & \text{for a disk and cylinder,}\\ (1+8\varphi)^{1/2}, & \text{for a sphere,}\end{cases} \tag{5.5}$$

where

$$\varphi = \begin{cases} k, & \text{for a disk,} \\ k\frac{1-\nu_{rz}\nu_{zr}}{1-\nu_{\theta z}\nu_{z\theta}}, & \text{for a cylinder,} \\ \frac{k-\nu_{\theta r}}{1-\nu_{\phi\theta}}, & \text{for a sphere.} \end{cases} \tag{5.6}$$

Consequently,

$$n_{1,2} = \begin{cases} 1 \mp \varphi^{1/2}, & \text{for a disk and cylinder,} \\ \frac{1}{2}[3 \mp (1+8\varphi)^{1/2}], & \text{for a sphere.} \end{cases} \tag{5.7}$$

In particular, for a uniform anisotropic disk, $n_{1,2} = 1 \mp k^{1/2}$. It is noted that the expressions $(5.7)_2$ are the correct expressions for the exponents $n_1$ and $n_2$ in the case of a sphere, and not those obtained from the expressions (52) and (53) of [16], which do not include the dependence on $\nu_{\phi\theta}$.

Having established the expression (5.1) for the radial stress, the circumferential stress follows from (4.1) as

$$\sigma_\theta = \left(1 - \frac{n_1}{j}\right) A r^{-n_1} + \left(1 - \frac{n_2}{j}\right) B r^{-n_2}. \tag{5.8}$$

The displacement is conveniently deduced from the circumferential strain as $u = r\epsilon_\theta$. By substituting (5.1) and (5.8) into the second of (2.1), the circumferential strain is found to be

$$\epsilon_\theta = \frac{1}{E_\theta^b}\left(\frac{b}{r}\right)^m \left(\eta_1 A r^{-n_1} + \eta_2 B r^{-n_2}\right), \tag{5.9}$$

with the parameters

$$\eta_1 = \gamma\left(1 - \frac{n_1}{j}\right) - \beta, \qquad \eta_2 = \gamma\left(1 - \frac{n_2}{j}\right) - \beta\,. \tag{5.10}$$

Therefore, the radial displacement is

$$u = \frac{b^m}{E_\theta^b}\left(\eta_1 A r^{1-m-n_1} + \eta_2 B r^{1-m-n_2}\right). \tag{5.11}$$

For isotropic homogeneous material, $\eta_1 = \gamma - \beta$ and $\eta_2 = -(\beta + \gamma/j)$, where $\beta$ and $\gamma$ are specified by (2.10). In general, $\eta_1 - \eta_2 = \gamma s/j$.

In the case of a thin disk under plane stress conditions ($\sigma_z = 0$), the strain in the direction orthogonal to the plane of the disk is $\epsilon_z = -(\nu_{zr}\sigma_r + \nu_{z\theta}\sigma_\theta)/E_z$, i.e., in view of the stress expressions (5.1) and (5.8),

$$-E_z\epsilon_z = [\nu_{zr} + (1-n_1)\nu_{z\theta}]A r^{-n_1} + [\nu_{zr} + (1-n_2)\nu_{z\theta}]B r^{-n_2}. \tag{5.12}$$

This is in general $r$-dependent, giving rise to the $r$-dependent out-of-plane displacement $w = z\epsilon_z(r)$, and thus the nonvanishing shear strain $\epsilon_{zr} = (z/2)\mathrm{d}\epsilon_z/\mathrm{d}r$, contrary to the initial plane stress assumption $\sigma_{zr} = 0$. This will be further discussed in Appendix A. The strain $\epsilon_z$ is $r$-independent if $n_1 = 0$ and $n_2 = 1 + \nu_{zr}/\nu_{z\theta} > 0$, or $n_2 = 0$ and $n_1 = 1 + \nu_{zr}/\nu_{z\theta} < 0$, provided that $m = 1 - (\nu_{zr}/\nu_{z\theta}) = (1-k)/(1-\nu_{\theta r})$. For example, this is the case for isotropic homogeneous material ($m = 0$, $k = 1$, $n_1 = 0$, $n_2 = 2$).

In the case of a long cylinder under plane strain conditions ($\epsilon_z = 0$), the longitudinal stress is $\sigma_z = \nu_{zr}\sigma_r + \nu_{z\theta}\sigma_\theta$. The generalized plane strain in which the longitudinal stress $\sigma_z = \sigma_z(r)$ is adjusted so that $\epsilon_z = \text{const.} \neq 0$ is considered in Appendix B.

### 5.1 Elaboration on the Exponents $n_1$ and $n_2$

The power-law radial dependence of stress components, embedded in (5.1) and (5.8), is specified by the exponents $n_1$ and $n_2$, which thus deserve a special attention. If $m > (1-\varphi)$, it can be readily verified from (5.2) that

$$(n_1 < 0, n_2 > 0). \tag{5.13}$$

If $m < (1-\varphi)$, then

$$\begin{cases} (n_1 > 0, n_2 > 0), & \text{for } m < (1+j), \\ (n_1 < 0, n_2 < 0), & \text{for } m > (1+j). \end{cases} \tag{5.14}$$

The second combination $(n_1 < 0, n_2 < 0)$, although possible in theory, may be difficult to achieve in practice. For example, for a disk with $m = 3, k = 1.25$, and $\nu_{\theta r} = 1.1$, we have that $n_1 < 0$ and $n_2 < 0$ without violating any of the required conditions, i.e., $k + m(1-\nu_{\theta r}) < 1$, $m^2 - 4m\nu_{\theta r} + 4k > 0$, $\nu_{\theta r} < k^{1/2}$, $k > 0$, and $m > 2$. In this case, $E_r(b) = 15.625E_r(a)$, with a similar relation for $E_\theta$. Such rapid stiffening of material with the distance is rather extreme. The case $(n_1 > 0, n_2 < 0)$ cannot occur, because $n_2 = n_1 + s$ and $s > 0$.

The explicit form of the condition $m > (1-\varphi)$ is

$$\begin{cases} k + m(1-\nu_{\theta r}) > 1, & \text{for a disk,} \\ k(1-\nu_{rz}\nu_{zr}) + m[1-\nu_{\theta r} - \nu_{\theta z}(\nu_{zr}+\nu_{z\theta})] + \nu_{\theta z}\nu_{z\theta} > 1, & \text{for a cylinder,} \\ k + m(1-\nu_{\theta r} - \nu_{\phi\theta}) + \nu_{\phi\theta} - \nu_{\theta r} > 1, & \text{for a sphere.} \end{cases} \tag{5.15}$$

The opposite inequalities hold in the case $m < (1-\varphi)$.

If $m = 1-\varphi$, then

$$\begin{cases} n_1 = 0,\ n_2 = 1 + j - m > 0, & \text{for } m < (1+j), \\ n_2 = 0,\ n_1 = 1 + j - m < 0, & \text{for } m > (1+j). \end{cases} \tag{5.16}$$

The condition $m = 1-\varphi$ implies that

$$\begin{cases} k = 1 - m(1-\nu_{\theta r}), & \text{for a disk,} \\ k = \frac{1}{1-\nu_{rz}\nu_{zr}}[(1-m)(1-\nu_{\theta z}\nu_{z\theta}) + m(\nu_{\theta r} + \nu_{\theta z}\nu_{zr})], & \text{for a cylinder,} \\ k = (1+m)\nu_{\theta r} + (1-m)(1-\nu_{\phi\theta}), & \text{for a sphere,} \end{cases} \tag{5.17}$$

provided that the right-hand side in each case is positive, and that (2.7)–(2.9) are obeyed.

The power-law dependence of the radial displacement (5.11) is specified by the exponents $(1-m-n_1)$ and $(1-m-n_2)$, so that the analysis of their physically possible values deserves a careful consideration. For example, for a particular combination of material parameters, the displacement at the center of a solid disk or sphere (without a hole) becomes singular. For a functionally graded disk this was examined in [11], where the displacement singularity was found at the center of the disk whose core is sufficiently soft.

## 6 Boundary Conditions

In this paper, only traction boundary conditions are considered. The solutions for the displacement or mixed-boundary conditions is presented in [24]. When the uniform pressures $p$ and $q$ are applied at the inner and outer boundary,

$$\sigma_r(a) = -p, \qquad \sigma_r(b) = -q, \tag{6.1}$$

the integration constants in (5.1) become

$$A = \frac{pc^{n_2} - q}{1 - c^s} b^{n_1}, \qquad B = \frac{pc^{n_1} - q}{1 - c^{-s}} b^{n_2}, \tag{6.2}$$

where $c = a/b$. Consequently, the radial and hoop stresses are

$$\sigma_r(r) = \frac{pc^{n_2} - q}{1 - c^s} \left(\frac{b}{r}\right)^{n_1} + \frac{pc^{n_1} - q}{1 - c^{-s}} \left(\frac{b}{r}\right)^{n_2}, \tag{6.3}$$

$$\sigma_\theta(r) = \left(1 - \frac{n_1}{j}\right) \frac{pc^{n_2} - q}{1 - c^s} \left(\frac{b}{r}\right)^{n_1} + \left(1 - \frac{n_2}{j}\right) \frac{pc^{n_1} - q}{1 - c^{-s}} \left(\frac{b}{r}\right)^{n_2}. \tag{6.4}$$

The corresponding radial displacement is

$$u(r) = \frac{b}{E_\theta^b} \left[ \eta_1 \frac{pc^{n_2} - q}{1 - c^s} \left(\frac{b}{r}\right)^{m+n_1-1} + \eta_2 \frac{pc^{n_1} - q}{1 - c^{-s}} \left(\frac{b}{r}\right)^{m+n_2-1} \right]. \tag{6.5}$$

Figure 1 shows the plots of the normalized stress components and the displacement versus the normalized radius in a hollow cylinder under plane strain ($j = 1$) with the radii ratio $c = a/b = 0.4$ and the loading ratio $q/p = 2$. It is assumed, for these and most subsequent plots in the paper, that the state of elastic anisotropy is such that $\alpha = 0.52$, $\beta = 0.304$, and $\gamma = 0.985$. These values correspond to the reported data for red oak (hardwood), for which $E_z = 9.8$ GPa, $E_r = 0.154E_z$, $E_\theta = 0.082E_z$ (thus $k = 0.532$), $\nu_{zr} = 0.35$, $\nu_{rz} = 0.064$, $\nu_{\theta r} = 0.292$, $\nu_{r\theta} = 0.56$, $\nu_{z\theta} = 0.448$, and $\nu_{\theta z} = 0.033$ [15]. The three curves shown in plots correspond to three indicated values of the nonuniformity parameter $m$. If $m = -0.25$, then $\varphi = 0.6051$, $n_1 = 0.3372$, and $n_2 = 1.9128$. The displacement parameters are $\eta_1 = 0.3489$ and $\eta_2 = -1.2032$. If $m = 0.25$, then $\varphi = 0.4508$, $n_1 = 0.1921$, and $n_2 = 1.5579$, while $\eta_1 = 0.4918$ and $\eta_2 = -0.8536$. If $m = 0$, then $\varphi = 0.5279$, $n_1 = 0.2734$, and $n_2 = 1.7266$, while $\eta_1 = 0.4117$ and $\eta_2 = -1.0197$. Part (a) of Fig. 1 shows the radial stress, part (b) the circumferential stress, and part (c) the radial displacement. The magnitude of the maximum circumferential stress $\sigma_\theta(a)$ for $m = -0.25$ is increased, and for $m = 0.25$ decreased relative to case of uniform material ($m = 0$). Different values of $m$ could be related to the age of wood, although no such correspondence is pursued in this paper, so that the selected values of $m$ are only chosen to illustrate the effect of material nonuniformity on the stress and displacement response. Recall that for the isotropic homogeneous disk or cylinder $\sigma_\theta(b) - \sigma_\theta(a) = q - p$.

Figure 2 shows the results for the pressure/tension loading $q = -p$. In the subsequent three sections a detailed analysis of the response is given in three important special cases, corresponding to the applied equal pressure at both boundaries, and the applied pressure at the inner or the outer boundary only. The appropriate superposition of the latter two cases can be used to obtain the solution for any loading combination.

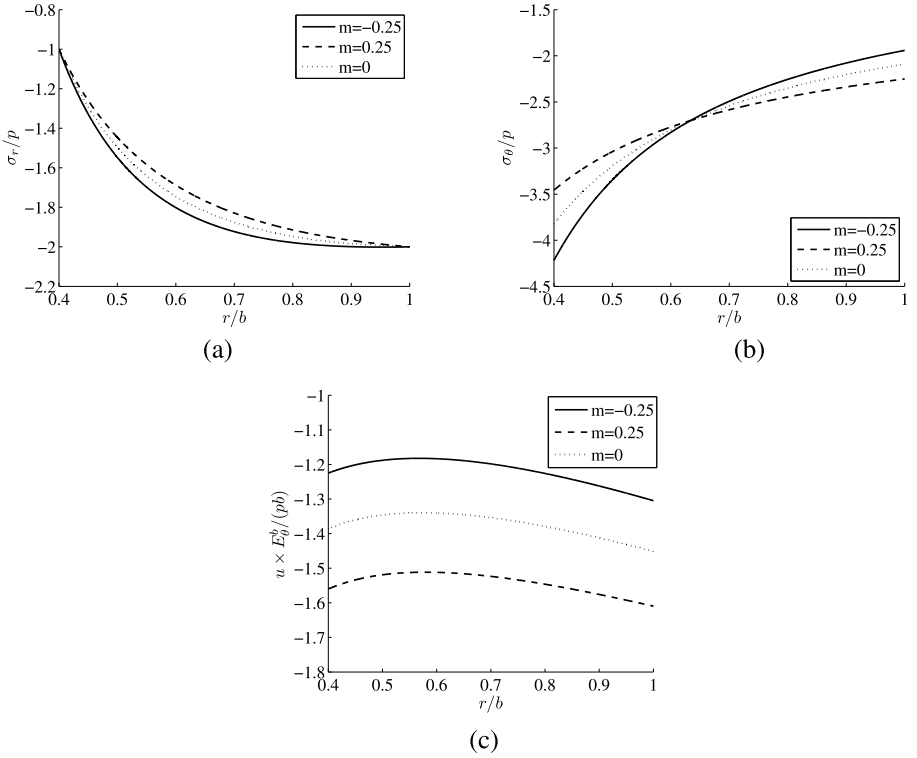


**Fig. 1** The variation of: (**a**) radial stress, (**b**) circumferential stress, and (**c**) radial displacement in the three cases described in the text. The aspect ratio is $c = a/b = 0.4$ and the loading is $q = 2p$

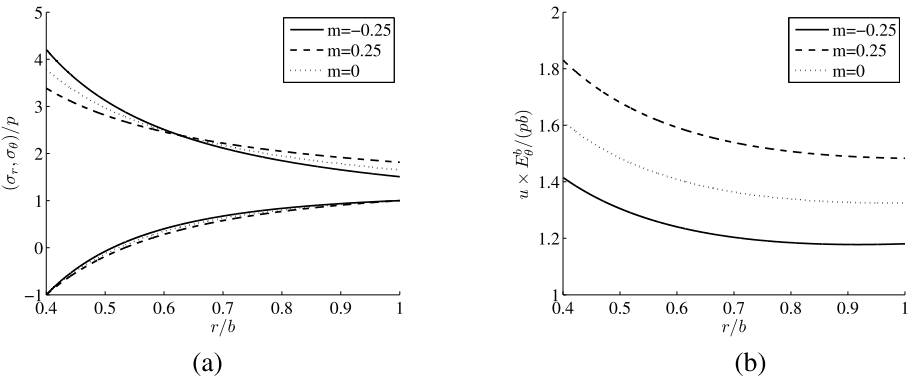


**Fig. 2** (**a**) The variation of the radial stress (*lower* three curves), and the circumferential stress (*upper* three curves) in the three considered cases for the pressure/tension loading $q = -p$. (**b**) The corresponding displacement variation

## 7 Response Under Equal Pressure at Both Boundaries

If the applied pressure is the same at both boundaries ($q = p$), the expressions for the radial and circumferential stresses (6.3) and (6.4) become

$$\sigma_r(r) = \left[\frac{c^{n_2}-1}{1-c^s}\left(\frac{b}{r}\right)^{n_1} + \frac{c^{n_1}-1}{1-c^{-s}}\left(\frac{b}{r}\right)^{n_2}\right]p, \tag{7.1}$$

$$\sigma_\theta(r) = \left[\left(1-\frac{n_1}{j}\right)\frac{c^{n_2}-1}{1-c^s}\left(\frac{b}{r}\right)^{n_1} + \left(1-\frac{n_2}{j}\right)\frac{c^{n_1}-1}{1-c^{-s}}\left(\frac{b}{r}\right)^{n_2}\right]p, \tag{7.2}$$

while the radial displacement (6.5) is

$$u(r) = \left[\eta_1\frac{c^{n_2}-1}{1-c^s}\left(\frac{b}{r}\right)^{m+n_1-1} + \eta_2\frac{c^{n_1}-1}{1-c^{-s}}\left(\frac{b}{r}\right)^{m+n_2-1}\right]\frac{pb}{E_\theta^b}. \tag{7.3}$$

In particular, if $n_1 = 0$ then $n_2 = s$; if $n_2 = 0$ then $n_1 = -s$. In both of these cases the state of anisotropy is such that $\varphi = 1 - m$, which requires that $m = 1 - (\alpha - j\beta)/(\gamma - \beta)$; see Sect. 5.1. The stress state throughout the disk/cylinder or sphere is then uniform and equal to $\sigma_r = \sigma_\theta = -p$. Furthermore, in both cases $\eta_1 = \eta_2 = \gamma - \beta$, so that the radial displacement is a nonlinear function of the radial coordinate $r$, given by

$$u(r) = u_b\left(\frac{b}{r}\right)^{m-1}, \quad u_b = (\beta - \gamma)\frac{pb}{E_\theta^b}. \tag{7.4}$$

If material is isotropic,

$$\gamma - \beta = \begin{cases} 1-\nu, & \text{for a disk,} \\ (1+\nu)(1-2\nu), & \text{for a cylinder,} \\ 1-2\nu, & \text{for a sphere,} \end{cases} \tag{7.5}$$

equation (7.4) reproduces the well-known displacement expression from the isotropic elasticity [29].

In neither $n_1$ nor $n_2$ vanish, the stress distribution is nonuniform. Figure 3 shows the stress and displacement variations for the same three cases of elastic anisotropy and nonuniformity as considered earlier in conjunction with Fig. 1. While the stress components are uniform in the case of isotropic uniform material, there is a strong nonuniformity of stress in cases of anisotropic or nonuniform material, which is particularly pronounced in magnitude for the circumferential stress.

If $a \ll b$, equation (7.2) gives

$$\frac{\sigma_\theta(a)}{p} \approx -\left(1-\frac{n_2}{j}\right) - \left(1-\frac{n_1}{j}\right)c^{-n_1}, \quad c = \frac{a}{b} \ll 1. \tag{7.6}$$

Consequently, if $n_1 < 0$ the circumferential stress $\sigma_\theta(a)$ approaches the value $-(1-n_2/j)p$. The magnitude of the circumferential stress $\sigma_\theta(a)$ is then less than $p$ (stress shielding) if $n_2 > 0$, and greater than $p$ if $n_2 < 0$. If $n_1 > 0$, the magnitude of $\sigma_\theta(a)$ increases in proportion to $(b/a)^{n_1}$ (stress amplification). In view of the analysis from Sect. 5.1, the combination $(n_1 < 0, n_2 > 0)$ occurs if $m > (1-\varphi)$. The combination $(n_1 < 0, n_2 < 0)$ occurs if $m < (1-\varphi)$ and $m > (1+j)$. The case $n_1 > 0$ occurs for $m < (1-\varphi)$ and $m < (1+j)$,

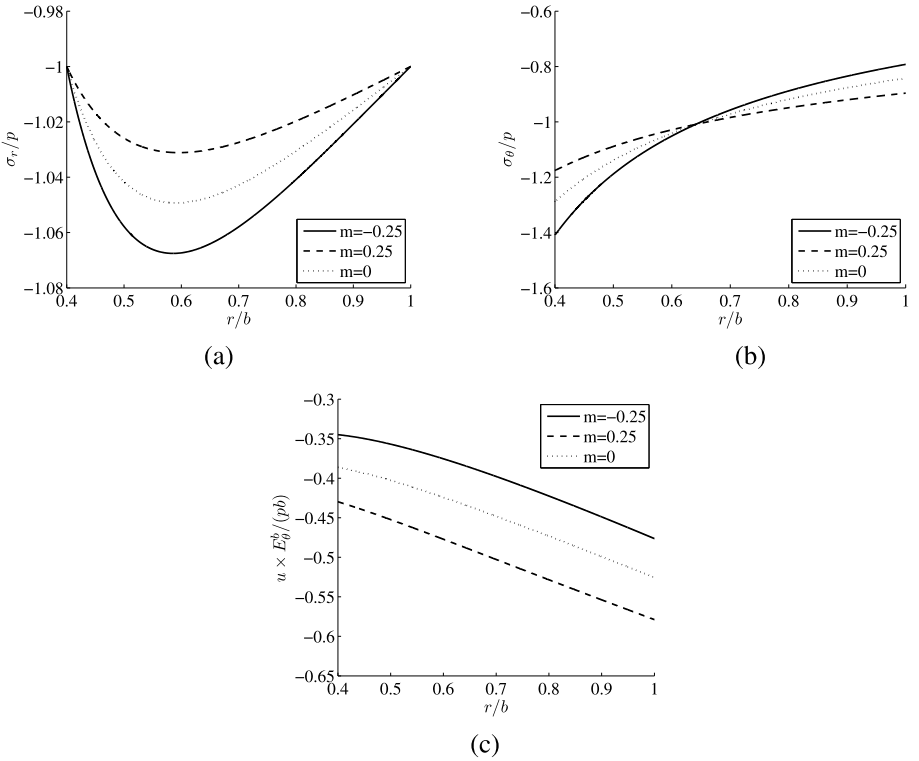


**Fig. 3** The variation of: (**a**) radial stress, (**b**) circumferential stress, and (**c**) radial displacement. The aspect ratio is $c = a/b = 0.4$ and the loading is $q = p$

and in this case $n_2$ is positive, as well. These cases can be achieved by various combinations of material nonuniformity and anisotropy parameters ($m$, $\alpha$, $\beta$, and $\gamma$), which is of interest for the optimization study [12].

As an illustration, for the uniform material ($m = 0$), the combination ($n_1 < 0, n_2 > 0$) occurs if

$$\begin{cases} k > 1, & \text{for a disk,} \\ k > \frac{1-\nu_{\theta z}\nu_{z\theta}}{1-\nu_{rz}\nu_{zr}}, & \text{for a cylinder,} \\ k > 1 + \nu_{\theta r} - \nu_{\phi\theta}, & \text{for a sphere.} \end{cases} \tag{7.7}$$

The combination ($n_1 < 0, n_2 < 0$) cannot occur for $m = 0$, while the case $n_1 > 0$ occurs if the direction of the inequalities in (7.7) is reversed.

Figure 4 shows the plots in the case $c = a/b = 0.01$, assuming the same state of elastic anisotropy and nonuniformity as in Fig. 2. For $m = -0.25$, the magnitude of the circumferential stress $\sigma_\theta(a)$ is equal to $6.5348p$ (stress amplification), for $m = 0$ it is $4.3966p$, and for $m = 0.25$ it is $2.7536p$. The magnitude of the maximum radial stress is everywhere greater than $p$, with the maximum of $2.8257p$ (for $m = -0.25$), $2.2337p$ (for $m = 0$), and $1.7065p$ (for $m = 0.25$).

It should be noted, however, that the results in Fig. 4, with the aspect ratio $a/b = 0.01$, give rise to $E_r(a) = 3.162E_r(b)$ in case $m = -0.25$, and $E_r(a) = 0.316E_r(b)$ in case $m = 0.25$. Such large difference in the elastic moduli at two boundaries may be rarely needed

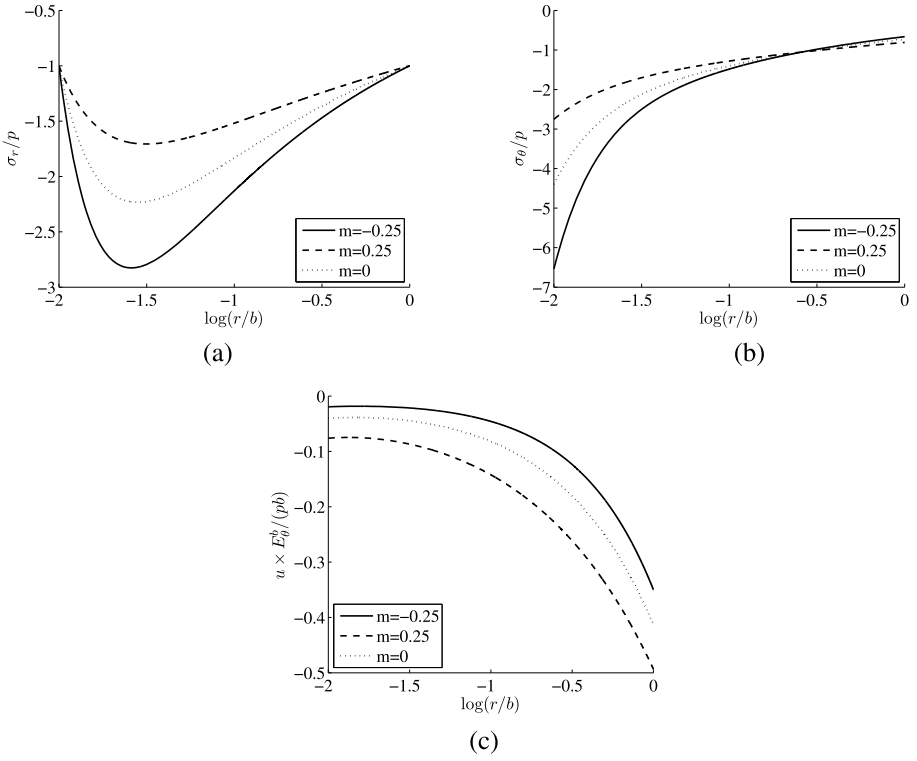


**Fig. 4** The variation of: (**a**) radial stress, (**b**) circumferential stress, and (**c**) radial displacement. The aspect ratio is $c = a/b = 0.01$ and the loading is $q = p$

or technologically produced by functional grading of the material. Furthermore, the state of elastic anisotropy at the inner boundary becomes profoundly concentrated (focussed) if $a = 0.01b$, which also gives rise to large stress amplification [16]. Since there is no material length scale in the problem, a minimum value of $a$ could be specified, below which the assumption of curvilinear anisotropy does not adequately apply.

In the case of a pressurized solid cylinder or sphere (without a central hole), there is a stress singularity at the origin caused by focusing of elastic anisotropy [21]. This has been addressed in great detail in [9], where it was observed that, near the center of a curvilinearly orthotropic cylinder with $k < 1$, there is an annular part ($kr_* < r < r_*$) in which the determinant of the deformation gradient ceases to be positive, implying a non one-to-one deformation mapping. In fact, in the small central core $r < r_*$ (the expression for $r_*$ can be found in [9]), the solution predicts $-u(r) > r$, which is physically impossible because it implies material interpenetration. The inequality $-u(r) > r$ means that the compressive circumferential strain is greater than 1, which is far beyond the range of infinitesimal strains assumed in classical linear elasticity. To remedy this situation, Fosdick and Royer-Carfagni [9] introduced the constraint of local injectivity, assuring local invertibility of the deformation mapping. The related analysis of a pressurized curvilinearly anisotropic solid sphere is reported in [1]. Furthermore, for a particular combination of material parameters, the displacement at the center of a solid disk can become singular. For a functionally graded disk obeying (3.1) with $m > 0$, this was examined in [11]. The problem was also considered in [27], where the

cylindrically orthotropic material of the inner core was replaced with a transversely isotropic material. The limitations of classical linear elasticity in problems which involve singularities around which the strains exceed the infinitesimal levels of linear theory have been discussed in a more general context by [2, 3, 10].

## 8 Response Under Internal Pressure

By substituting $q = 0$ in the general expressions (6.3)–(6.5), the stresses are found to be

$$\sigma_r(r) = \left[\frac{c^s}{1-c^s}\left(\frac{a}{r}\right)^{n_1} - \frac{1}{1-c^s}\left(\frac{a}{r}\right)^{n_2}\right]p, \tag{8.1}$$

$$\sigma_\theta(r) = \left[\left(1-\frac{n_1}{j}\right)\frac{c^s}{1-c^s}\left(\frac{a}{r}\right)^{n_1} - \left(1-\frac{n_2}{j}\right)\frac{1}{1-c^s}\left(\frac{a}{r}\right)^{n_2}\right]p. \tag{8.2}$$

The radial displacement is

$$u(r) = \left[\eta_1\frac{c^s}{1-c^s}\left(\frac{a}{r}\right)^{m+n_1-1} - \eta_2\frac{1}{1-c^s}\left(\frac{a}{r}\right)^{m+n_2-1}\right]\frac{pa}{E_\theta^a}. \tag{8.3}$$

Figure 5 shows the plots in the case $c = 0.4$, assuming the same states of elastic anisotropy and nonuniformity as in previous figures.

If $n_1 = 0$ then $n_2 = s$, and the stress and displacement fields become

$$\sigma_r(r) = \frac{c^s}{1-c^s}\left[1-\left(\frac{b}{r}\right)^s\right]p, \tag{8.4}$$

$$\sigma_\theta(r) = \frac{c^s}{1-c^s}\left[1-\left(1-\frac{s}{j}\right)\left(\frac{b}{r}\right)^s\right]p, \tag{8.5}$$

$$u(r) = (\gamma-\beta)\frac{c^s}{1-c^s}\left[1-\left(\frac{b}{r}\right)^s\right]\left(\frac{b}{r}\right)^{m-1}\frac{pb}{E_\theta^b}. \tag{8.6}$$

On the other hand, if $n_2 = 0$ then $n_1 = -s$, and

$$\sigma_r(r) = \frac{1}{c^s-1}\left[1-\left(\frac{r}{b}\right)^s\right]p, \tag{8.7}$$

$$\sigma_\theta(r) = \frac{1}{c^s-1}\left[1-\left(1+\frac{s}{j}\right)\left(\frac{r}{b}\right)^s\right]p, \tag{8.8}$$

$$u(r) = (\gamma-\beta)\frac{1}{c^s-1}\left[1-\left(\frac{r}{b}\right)^s\right]\left(\frac{b}{r}\right)^{m-1}\frac{pb}{E_\theta^b}. \tag{8.9}$$

If $a \ll b$, (8.1)–(8.3) reduce to

$$\sigma_r(r) \approx \left(\frac{a}{r}\right)^{n_2}\left[\left(\frac{r}{b}\right)^s - 1\right]p, \tag{8.10}$$

$$\sigma_\theta(r) \approx \left(\frac{a}{r}\right)^{n_2}\left[\left(1-\frac{n_1}{j}\right)\left(\frac{r}{b}\right)^s - \left(1-\frac{n_2}{j}\right)\right]p, \tag{8.11}$$

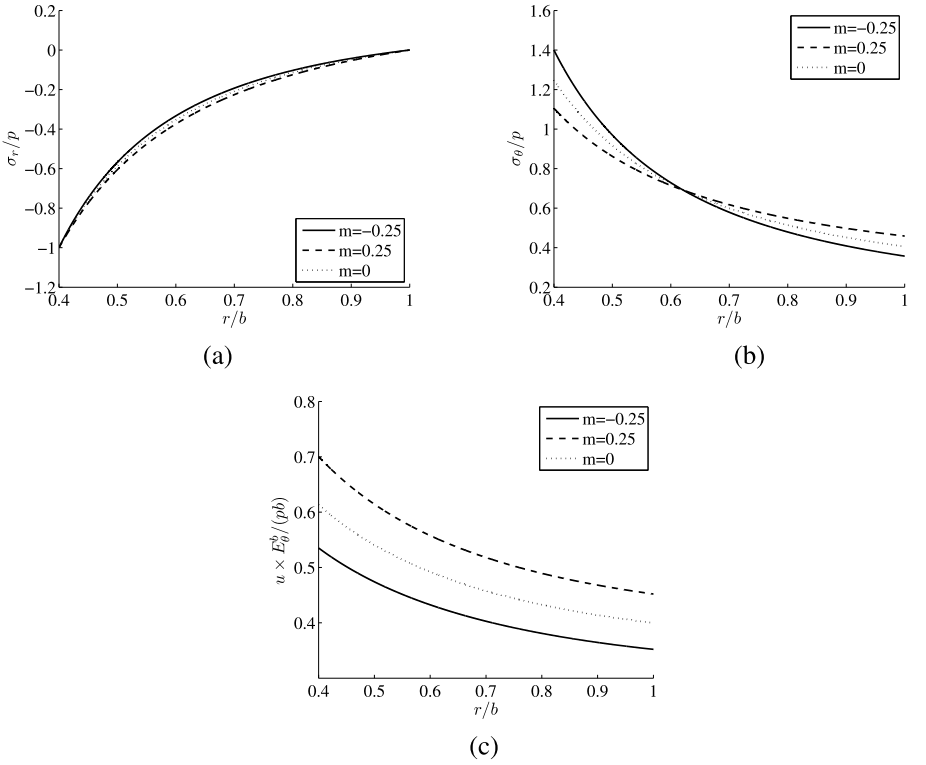


**Fig. 5** The variation of: (**a**) radial stress, (**b**) circumferential stress, and (**c**) radial displacement under internal pressure alone ($q = 0$). The aspect ratio is $c = a/b = 0.4$

$$u(r) \approx \left(\frac{a}{r}\right)^{m+n_2-1}\left[\eta_1\left(\frac{r}{b}\right)^s - \eta_2\right]\frac{pa}{E_\theta^a}. \tag{8.12}$$

The circumferential stress at two boundaries is then

$$\sigma_\theta(a) \approx -\left(1 - \frac{n_2}{j}\right)p, \qquad \sigma_\theta(b) = \frac{s}{j}\left(\frac{a}{b}\right)^{n_2} p. \tag{8.13}$$

Thus, if $n_2 > 0$, the magnitude of $\sigma_\theta(a)$ is less than $p$, while $\sigma_\theta(b) \ll p$. Dually, if $n_2 < 0$, the magnitude of $\sigma_\theta(a)$ is greater than $p$, while $\sigma_\theta(b) \gg p$ (stress amplification). Figure 6 shows the results for $a = 0.01b$, demonstrating a rapid decrease of both radial and circumferential stress away from the inner radius $r = a$. Adding more material beyond a sufficiently large radius, in the case of the considered material parameters, barely affects the stress state near the pressurized hole. The displacement at the inner radius is $u(a) \approx -\eta_2 c^{1-m}(p/E_\theta^b)$, with $-\eta_2 = (1.2032, 1.0197, 0.8536)$ for $m = (-0.25, 0, 0.25)$, respectively.

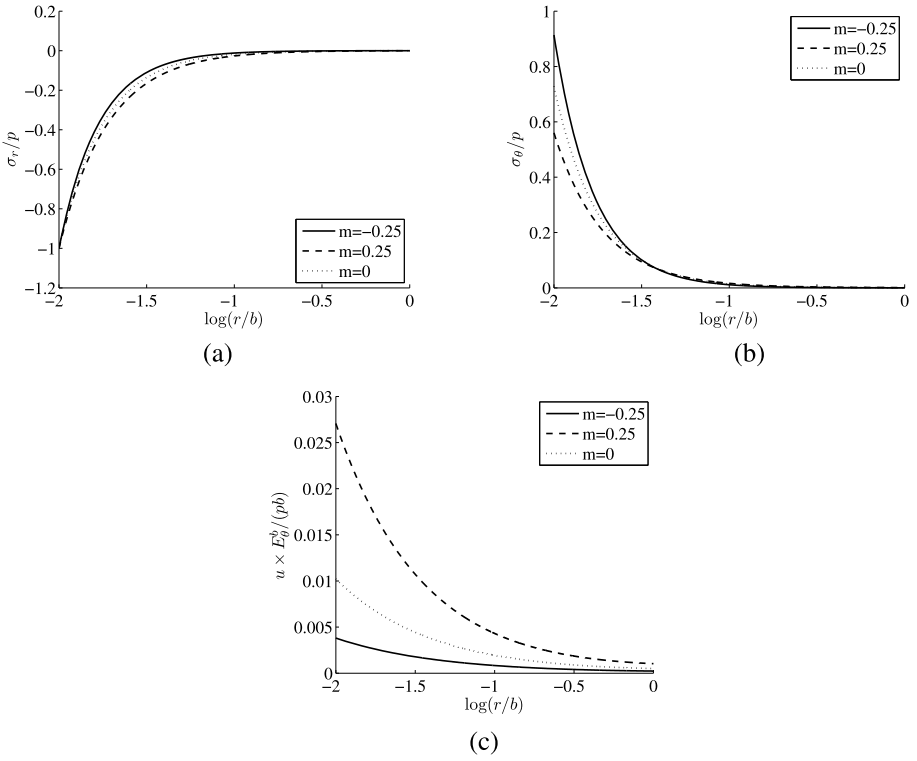


**Fig. 6** The variation of: (**a**) radial stress, (**b**) circumferential stress, and (**c**) radial displacement under internal pressure alone ($q = 0$). The aspect ratio is $c = a/b = 0.01$

## 9 Response Under External Pressure

If $p = 0$ is substituted in (6.3)–(6.5), the stresses become

$$\sigma_r(r) = \left[\frac{1}{c^s - 1}\left(\frac{b}{r}\right)^{n_1} + \frac{c^s}{1 - c^s}\left(\frac{b}{r}\right)^{n_2}\right]q, \tag{9.1}$$

$$\sigma_\theta(r) = \left[\left(1 - \frac{n_1}{j}\right)\frac{1}{c^s - 1}\left(\frac{b}{r}\right)^{n_1} + \left(1 - \frac{n_2}{j}\right)\frac{c^s}{1 - c^s}\left(\frac{b}{r}\right)^{n_2}\right]q. \tag{9.2}$$

The radial displacement is

$$u(r) = \left[\eta_1\frac{1}{c^s - 1}\left(\frac{b}{r}\right)^{m+n_1-1} + \eta_2\frac{c^s}{1 - c^s}\left(\frac{b}{r}\right)^{m+n_2-1}\right]\frac{qb}{E_\theta^b}. \tag{9.3}$$

Figure 7 shows the stress and displacement variations for $a = 0.4b$, in the same three cases of material anisotropy and nonuniformity as before.

If $n_1 = 0$ then $n_2 = s$, and the stress and displacement fields are

$$\sigma_r(r) = \frac{1}{c^s - 1}\left[1 - \left(\frac{a}{r}\right)^s\right]q, \tag{9.4}$$

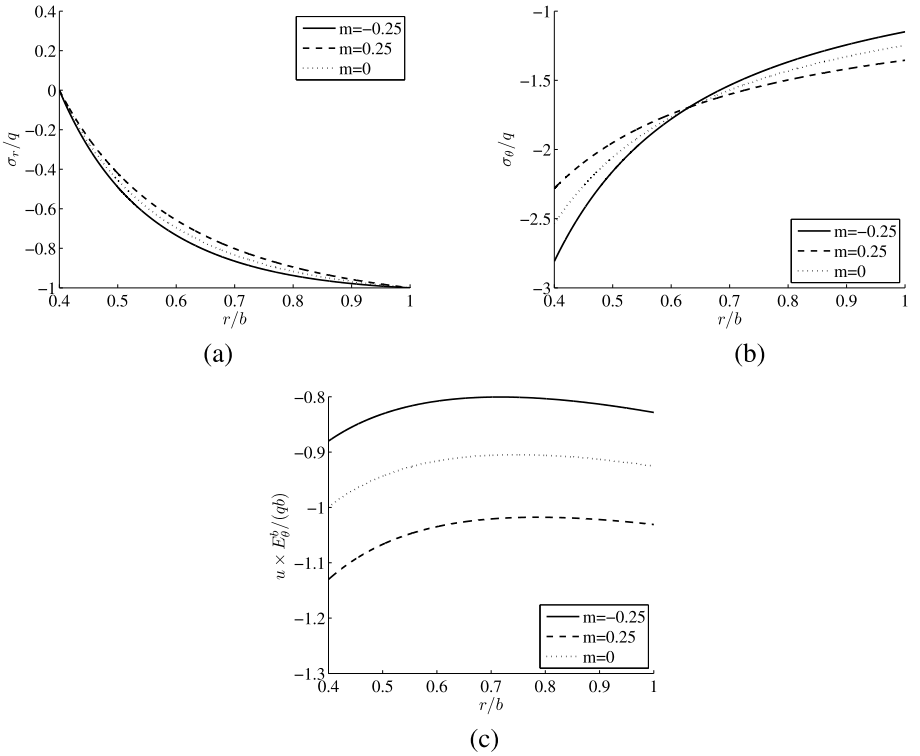


**Fig. 7** The variation of: (**a**) radial stress, (**b**) circumferential stress, and (**c**) radial displacement under external pressure alone ($p = 0$). The aspect ratio is $c = a/b = 0.4$

$$\sigma_\theta(r) = \frac{1}{c^s - 1}\left[1 - \left(1 - \frac{s}{j}\right)\left(\frac{a}{r}\right)^s\right]q, \tag{9.5}$$

$$u(r) = (\gamma - \beta)\,\frac{1}{c^s - 1}\left[1 - \left(\frac{a}{r}\right)^s\right]\left(\frac{a}{r}\right)^{m-1}\frac{qa}{E_\theta^a}. \tag{9.6}$$

Thus,

$$\frac{\sigma_\theta(a)}{\sigma_r(b)} = \frac{s/j}{1 - (a/b)^s}, \tag{9.7}$$

so that, in the limit as $b \gg a$, the stress concentration factor becomes equal to $s/j$. Since $n_1 = 0$, one has $s = 1 + j - m$, so that the stress concentration factor can also be expressed as $1 + (1 - m)/j$. For a uniform and isotropic material, the stress concentration factor is $(1 + 1/j)$, which is equal to 2 for a disk or cylinder, and 1.5 for a sphere.

On the other hand, if $n_2 = 0$ then $n_1 = -s$, and the stress and displacement fields are

$$\sigma_r(r) = \frac{c^s}{1 - c^s}\left[1 - \left(\frac{r}{a}\right)^s\right]q, \tag{9.8}$$

$$\sigma_\theta(r) = \frac{c^s}{1 - c^s}\left[1 - \left(1 + \frac{s}{j}\right)\left(\frac{r}{a}\right)^s\right]q, \tag{9.9}$$

$$u_r(r) = (\gamma - \beta)\,\frac{c^s}{1-c^s}\left[1 - \left(\frac{r}{a}\right)^s\right]\left(\frac{a}{r}\right)^{m-1}\frac{qa}{E_\theta^a}. \tag{9.10}$$

In this case,

$$\frac{\sigma_\theta(a)}{\sigma_r(b)} = \frac{s/j}{(b/a)^s - 1}, \tag{9.11}$$

which decreases with the increase of the ratio $b/a$. If $b \gg a$, the stress concentration factor approaches 0, which has been referred to as the stress shielding effect by curvilinear anisotropy of radial nonuniformity of the material [13, 17]. It is noted that the derived expressions in [13] for $m = 0$ correspond to anisotropic thin disks under plane stress, rather than thick cylinders under plane strain conditions, as stated in that paper. The stresses are fundamentally different in two cases: for a thin disk they depend on the ratio $E_\theta/E_r$, but not on the coefficients of lateral contraction, while for a thick cylinder they depend on both; see (5.6). For isotropic material they are, of course, independent of material properties.

The stress shielding, or the stress amplification, can occur for various combinations of the anisotropy and nonuniformity parameters, as represented by the parameter $n_1$. In fact, from (9.2),

$$\frac{\sigma_\theta(a)}{q} = \frac{s}{j}\frac{c^{-n_1}}{c^s - 1}. \tag{9.12}$$

Furthermore, from (9.3), the normalized inward displacement of the points at the surface of the inner hole is

$$-\frac{u(a)}{a} = \frac{\gamma s/j}{1-c^s}c^{-(n_1+m)}\frac{q}{E_\theta^b}, \qquad n_1 + m = \frac{1}{2}(1 + j + m - s). \tag{9.13}$$

Since $s > 0$, for $c \ll 1$, (9.12) and (9.13) become

$$\frac{\sigma_\theta(a)}{q} \approx -\frac{s}{j}\,c^{-n_1}, \qquad -\frac{u(a)}{a} = \frac{\gamma s}{j}c^{-(n_1+m)}\frac{q}{E_\theta^b}. \tag{9.14}$$

Consequently, if $n_1 < 0$ the stress concentration factor diminishes to zero (stress shielding); if $n_1 > 0$, the stress concentration factor increases to infinity (stress amplification). If $n_1 = 0$, the stress concentration factor approaches the value $s/j$, as discussed earlier. Furthermore, the material interpenetration, in the sense of [9, 11], does not occur if $n_1 + m < 0$, i.e., $m < s - (1 + j)$. For example, the interpenetration cannot occur in isotropic radially nonuniform cylinder if $m < 0$, for then $-u(a)/a \to 0$ as $c \to 0$.

Figure 8 shows the plots for $c = 0.01$. The magnitude of $\sigma_r$ in case $m = -0.25$ is increased and in case $m = 0.25$ decreased, relative to case $m = 0$. The circumferential stress at the inner radius in case $m = -0.25$ is $\sigma_\theta(a) = -7.4488q$ (stress amplification), while in case $m = 0.25$ it is $\sigma_\theta(a) = -3.3141q$ (stress shielding), as compared to $\sigma_\theta(a) = -5.125q$ in the case of uniform material ($m = 0$).

Physically, the stress amplification can be explained by considering separately the cases of isotropic nonuniform material, and anisotropic uniform material. In the case of isotropic nonuniform disk/cylinder or sphere, the condition $n_1 > 0$ implies $m < 0$ (i.e., material stiffening inwards). Thus, if $E_r^b$ is finite, the elastic modulus $E_r^a$ increases indefinitely as the inner radius $a$ decreases. Such infinite stiffness is physically unrealistic, which implies that the radial nonuniformity model (5.2) is physically meaningful only for $r \geq a_0$, where $a_0$ is a cut-off, minimal permissible radius of the inner hole, specified by the production process

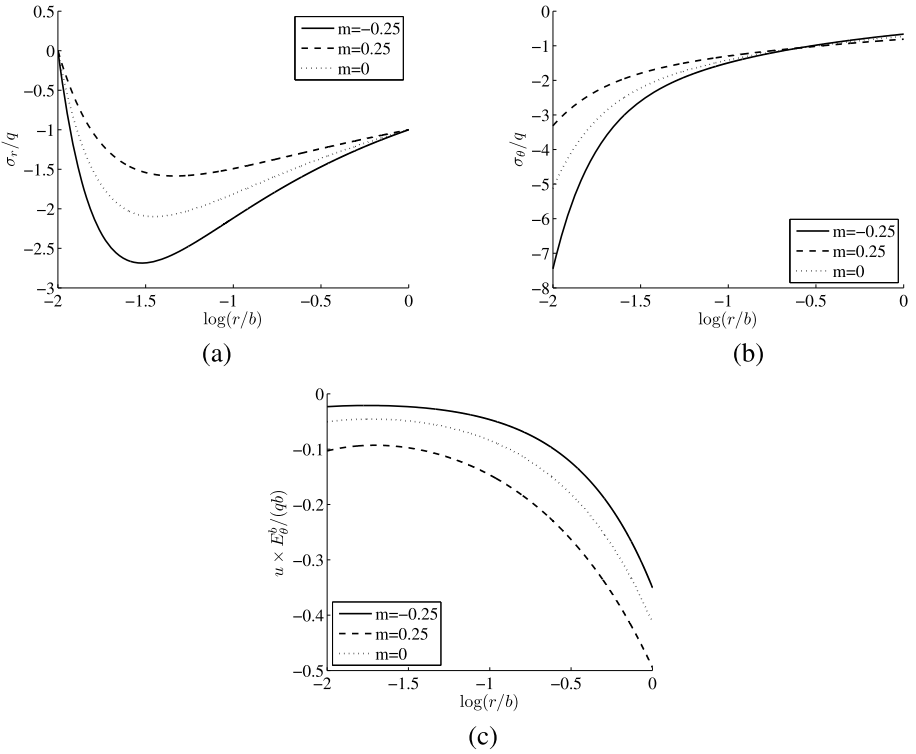


**Fig. 8** The variation of: (**a**) radial stress, (**b**) circumferential stress, and (**c**) radial displacement under external pressure alone ($p = 0$). The aspect ratio is $c = a/b = 0.01$

of the disk/cylinder or the sphere. Even then, depending on the value of $m$, linear elasticity may predict the stress and displacement near the core that are beyond the range of linear theory. Alternatively, if $a$ and $E_r^a$ are specified, the elastic modulus $E_r^b$ decreases indefinitely as the outer radius $b$ increases. Such infinitesimally small stiffness at the outer boundary is also physically unrealistic, giving rise to unrealistic infinite stress amplification at the inner radius.

In the case of anisotropic uniform disk, the condition $n_1 > 0$ implies $k < 1$, i.e., $E_r > E_\theta$. Thus, the unbounded stress amplification occurs at the inner radius $a \ll b$ due to physically unrealistic concentration (focusing) of anisotropy near the inner radius, in which the radial stiffness is greater than the circumferential stiffness. One cannot produce the material that so rapidly changes the properties in the same direction, i.e., for sufficiently small $a$, the modulus $E_r(a)$ at $\theta = 0$ should be nearly equal to $E_\theta(a)$ at $\theta = \pi/2$. In the case of anisotropic uniform cylinder, the condition $n_1 > 0$ implies $k < (1 - \nu_{\theta z}\nu_{z\theta})/(1 - \nu_{rz}\nu_{zr})$, and in the case of a sphere, $k < (1 + \nu_{\theta r} - \nu_{\theta\phi})$.

The comment should also be made regarding the lack of asymptotic value of the stress concentration factor $\sigma_\theta(a)/q$ in the limit $a \ll b$, previously discussed in [13, 16]. While in the uniform isotropic case this stress concentration factor is $1 + (1/j)$, it clearly does not have an asymptotic limit in the case of either nonuniform or anisotropic material, because the sequence of disks/cylinders or spheres with the increasing ratio $b/a$ constitute different structural problems: material with different elastic properties is added to obtain a new member of the sequence (with different magnitude of the isotropic moduli in the case of isotropic

nonuniform material, or different magnitude of the concentration of anisotropy in the case of uniform anisotropic material).

## 10 Conclusion

An analysis of the elastic response of a pressurized cylindrically anisotropic hollow disk or hollow cylinder, and a spherically anisotropic hollow sphere, made of material which is nonuniform in the radial direction according to the power law relationship, is presented. Two parameters play a prominent role in the analysis: the material nonuniformity parameter $m$, and the parameter $\varphi$ which accounts for the combined effects of material anisotropy and material nonuniformity. The radial and circumferential stresses are shown to be the linear combinations of two power functions of the radial coordinate, whose exponents depend on the material parameters $m$ and $\varphi$. The stress amplification or shielding effects are quantitatively and qualitatively examined in the presence of both, curvilinear anisotropy and radial nonuniformity. The effects of the material parameters on the displacement response are also analyzed. The approximate character of the plane stress solution of a pressurized thin disk is discussed in the Appendix A. It is shown that for a mildly nonuniform and isotropic thin disk the plane stress model delivers accurate values for the radial and circumferential stress components, although it does not account for small out-of-plane stress components present in the three-dimensional disk model. Appendix B offers an analysis of a pressurized long cylinder under conditions of generalized plane strain. The obtained results may be of interest for the tailoring of material properties, optimization studies and processing of curvilinearly anisotropic and functionally graded materials.

**Acknowledgements** This research was supported by the Montenegrin Academy of Sciences and Arts. Valuable comments and suggestions by Professor Adair Aguiar from the University of Sao Paulo, Brazil, are gratefully acknowledged.

## Appendix A: Evaluation of the Plane Stress Approximation

In general, the solution of plane stress problems in linear isotropic elasticity are only approximate. The assumption that the in-plane stresses do not depend on the $z$-coordinate, while the out-of-plane stresses identically vanish, cannot be satisfied exactly, because some of the compatibility conditions remain unsatisfied. The full solution in the framework of three-dimensional isotropic elasticity [29] allows the in-plane stresses to depend on the $z$-coordinate, while the out-of-plane stresses all vanish. The correction terms in this exact theory are proportional to $z^2$, where $z$ is measured from the midsurface of the disk, and are thus negligibly small for very thin disks. In the case of the Lamé problem of a pressurized isotropic disk, the plane stress solution is the exact solution, because the sum $\sigma_r + \sigma_\theta$ turns out to be constant throughout the disk, so that $\epsilon_z$ $(= \epsilon_z^0)$ is also constant (the disk having uniform thickness in the deformed configuration, as well). As a consequence, all Saint-Venant compatibility conditions are identically satisfied by the displacement field $u = Ar + B/r$, $v = 0$, and $w = \epsilon_z^0 z$.

The situation is quite different with the Lamé problem of a radially nonuniform and/or cylindrically anisotropic disk. The assumption $u = u(r)$, together with the vanishing out-of-plane stresses ($\sigma_{zz} = \sigma_{zr} = 0$), gives rise to in-plane stresses ($\sigma_r$, $\sigma_\theta$) dependent on $r$ only, and thus, from Hooke's law, the strain $\epsilon_z = \epsilon_z(r)$, so that the out-of-plane displacement

$w = z\epsilon_z(r)$ is linear in $z$, but, in general, nonlinear in $r$. For example, from (5.12) it follows that for a uniform cylindrically orthotropic disk,

$$w = -\frac{1}{E_z}\left[(\nu_{zr} + \sqrt{k}\nu_{z\theta})Ar^{-1+\sqrt{k}} + (\nu_{zr} - \sqrt{k}\nu_{z\theta})Br^{-1-\sqrt{k}}\right]z. \tag{A.1}$$

This, in turn, implies that the shear strain

$$\epsilon_{zr} = \frac{1}{2}\left(\frac{\partial u}{\partial z} + \frac{\partial w}{\partial r}\right) = \frac{z}{2}\frac{\mathrm{d}\epsilon_z}{\mathrm{d}r} \neq 0, \tag{A.2}$$

contrary to the initial assumption that the shear stress component $\sigma_{zr} = 2G_{zr}\epsilon_{zr} = 0$. This is reminiscent to the nature of approximation involved in the Euler-Bernoulli beam theory, or the Kirchhoff thin plate theory [35]. We thus present bellow an exact elasticity formulation for a pressurized radially nonuniform and cylindrically anisotropic disk. In Sect. A.1 we numerically solve the governing partial differential equations in the case of a radially nonuniform isotropic disk and discuss the accuracy of the plane stress disk modeling.

The displacement components in the full three-dimensional axisymmetric analysis of a pressurized disk are

$$u = u(r, z), \qquad v = 0, \qquad w = w(r, z). \tag{A.3}$$

The associated non-vanishing strain components are

$$\epsilon_r = \frac{\partial u}{\partial r}, \qquad \epsilon_\theta = \frac{u}{r}, \qquad \epsilon_z = \frac{\partial w}{\partial z}, \qquad \epsilon_{zr} = \frac{1}{2}\left(\frac{\partial u}{\partial z} + \frac{\partial w}{\partial r}\right). \tag{A.4}$$

The two independent Saint-Venant's compatibility equations are

$$\begin{aligned} r\frac{\partial \epsilon_\theta}{\partial r} + \epsilon_\theta - \epsilon_r &= 0, \\ r\frac{\partial^2 \epsilon_\theta}{\partial z^2} + \frac{\partial \epsilon_z}{\partial r} - 2\frac{\partial \epsilon_{zr}}{\partial z} &= 0. \end{aligned} \tag{A.5}$$

The remaining Saint-Venant's compatibility equation is identically satisfied if equations in (A.5) are satisfied, because

$$\frac{\partial^2 \epsilon_r}{\partial z^2} + \frac{\partial^2 \epsilon_z}{\partial r^2} - 2\frac{\partial^2 \epsilon_{zr}}{\partial r \partial z} = \frac{\partial L_r}{\partial r} - \frac{\partial^2 L_z}{\partial z^2} = 0. \tag{A.6}$$

where $L_z$ and $L_r$ stand for the left-hand sides of expressions in (A.5).

The non-vanishing stresses are $\sigma_r = \sigma_r(r, z)$, $\sigma_\theta = \sigma_\theta(r, z)$, $\sigma_z = \sigma_z(r, z)$, and $\sigma_{zr} = \sigma_{zr}(r, z)$. In particular, by symmetry across the mid-plane $z = 0$ of the disk, the normal stress $\sigma_z$ must be an even, while the shear stress $\sigma_{zr}$ must be an odd function of $z$ (its average value over the height $h$ of the disk thus being equal to zero). The equilibrium equations in the $r$ and $z$ direction are

$$\begin{aligned} \frac{\partial \sigma_r}{\partial r} + \frac{1}{r}(\sigma_r - \sigma_\theta) + \frac{\partial \sigma_{zr}}{\partial z} &= 0, \\ \frac{\partial \sigma_{zr}}{\partial r} + \frac{1}{r}\sigma_{zr} + \frac{\partial \sigma_z}{\partial z} &= 0. \end{aligned} \tag{A.7}$$

In particular, the second equilibrium equation in (A.7) yields an expression for the normal stress

$$\sigma_z = -\frac{1}{r}\frac{\partial}{\partial r}\left(r\int_z^{h/2}\sigma_{zr}\,\mathrm{d}z\right). \tag{A.8}$$

Since $\sigma_{zr}(r,\pm h/2)=0$ and $\sigma_{zr}(r,0)=0$, from the second of (A.7) it follows that $\partial\sigma_z/\partial z = 0$ over the planes $z=0$ and $z=\pm h/2$. Thus, since $\sigma_z = \partial\sigma_z/\partial z = 0$ at $z=\pm h/2$, it may be expected that $\sigma_z$ does not significantly build over the small thickness of the disk, as confirmed by the numerical analysis in Sect. A.1. The boundary conditions of the problem are

$$\begin{aligned} &\sigma_z(r,\pm h/2)=0, \qquad &&\sigma_{zr}(r,\pm h/2)=0,\\ &\sigma_r(a,z)=-p, \qquad &&\sigma_{zr}(a,z)=0,\\ &\sigma_r(b,z)=-q, \qquad &&\sigma_{zr}(b,z)=0. \end{aligned} \tag{A.9}$$

## A.1 Numerical Solution

To quantify the approximation involved in the plane stress modeling of the disk, we present in this section a numerical solution of the formulated three-dimensional disk problem in the case of a radially nonuniform isotropic disk. The governing differential equations for the displacement components $(u,w)$ are obtained by substituting the strain-displacement relations (A.4) and the stress-strain relations

$$\sigma_r = \frac{E(r)}{(1+\nu)(1-2\nu)}\big[(1-\nu)\epsilon_r+\nu(\epsilon_\theta+\epsilon_z)\big], \qquad \sigma_{zr}=\frac{E(r)}{1+\nu}\epsilon_{zr}, \tag{A.10}$$

with the similar relations for $\sigma_\theta$ and $\sigma_z$, into the equilibrium equations (A.7). This gives a coupled system of two second-order partial differential equations

$$\begin{aligned} &\frac{1}{2}r\left[2(1-\nu)\frac{\partial^2 u}{\partial r^2}+(1-2\nu)\frac{\partial^2 u}{\partial z^2}+\frac{\partial^2 w}{\partial r\,\partial z}\right]\\ &\quad+(1-\nu)(1+m)\frac{\partial u}{\partial r}+\nu m\frac{\partial w}{\partial z}-\big[1-\nu(1+m)\big]\frac{u}{r}=0, \end{aligned} \tag{A.11}$$

$$\begin{aligned} &r\left[\frac{\partial^2 u}{\partial r\,\partial z}+(1-2\nu)\frac{\partial^2 w}{\partial r^2}+2(1-\nu)\frac{\partial^2 w}{\partial z^2}\right]\\ &\quad+\big[1+(1-2\nu)m\big]\frac{\partial u}{\partial z}+(1-2\nu)(1+m)\frac{\partial w}{\partial r}=0. \end{aligned} \tag{A.12}$$

Equations (A.11) and (A.12) are solved numerically by using the finite difference method. Due to symmetry, the finite difference mesh was applied to rectangular region $a\le r\le b$, $0\le z\le h/2$, where $h$ is the thickness of the disk. The boundary conditions $w=\partial u/\partial z=0$ are imposed along the side $z=0$, and the boundary conditions associated with the prescribed traction are imposed along the other three sides. Figure 9 shows the variation of the displacement components along the vertical section $r=(b-a)/2$ and the horizontal section $z=h/4$ in a disk of thickness $h=a/10$ and external radius $b=2.5a$, under applied tension $q$ at the outer boundary $r=b$. The nonuniformity parameter is taken to be $m=0.5$, so that $E(b)\approx 1.58E(a)$. The solid curves show the results obtained by using the central finite differences to solve the differential equations (A.11) and (A.12), while the dashed curves correspond to calculations based on the plane stress modeling. The numerical

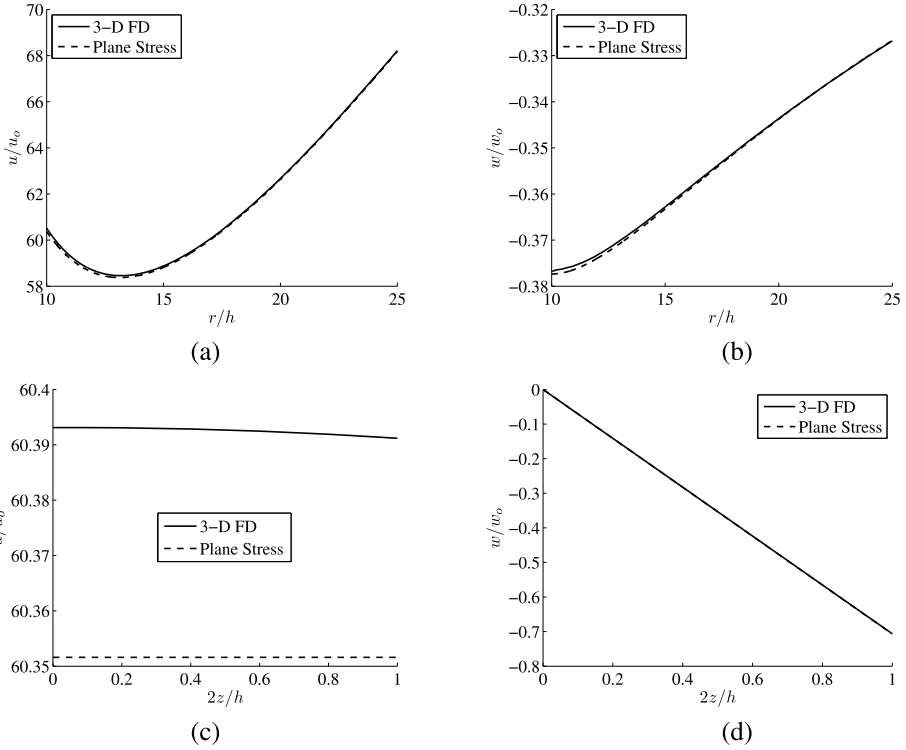


**Fig. 9** The variation of the (**a**) radial, and (**b**) vertical displacement along the horizontal section $z = h/4$ of a thin disk with $b = 2.5a = 25h$ and $m = 0.5$. Parts (**c**) and (**d**) show the same along the vertical section $r = (b - a)/2$. The normalizing displacement is $u_o = w_o = qh/E_b$, where $q$ is the applied tension at $r = b$, and $E_b = E(b)$

accuracy was verified by choosing a sufficiently fine mesh density ($900 \times 30$), and by the agreement of the results with the exact analytical solution available in the case of a uniform disk. The vertical displacement in the exact formulation is almost linear across the height of the disk, albeit with a slightly different slope from that predicted by the plane stress approximation. The radial displacement is only mildly dependent on $z$, and on the scale of Fig. 9c it can hardly be observed. The corresponding variations of the radial and hoop stress components with the radius $r$ are shown in Fig. 10. Their variation with $z$, based on the finite difference calculation, is not shown, because it is exceedingly small, so that $\sigma_r$ and $\sigma_\theta$ are in this case nearly constant across the height of the disk. The out-of-plane normal stress ($\sigma_z$) and the shear stress ($\sigma_{zr}$) are much smaller than the applied stress $q$, particularly away from the ends of the disk, with the maximum values of the order of $10^{-4}q$.

For a given geometry of the disk (thickness to radii ratios), the agreement between the three-dimensional and the plane stress calculations depends on the value of the nonuniformity parameter $m$ (its magnitude and the sign), as well as the loading combination. For example, Fig. 11 shows the plots for the radial and circumferential stresses in the disk ($b = 2.5a = 25h$) under external pressure when $m = 2$, so that $E(b) = 6.25E(a)$. Note that in this case the maximum hoop stress occurs at $r = b$, rather than $r = a$, because of significantly increased material stiffness of the outer portion of the disk. The stress components

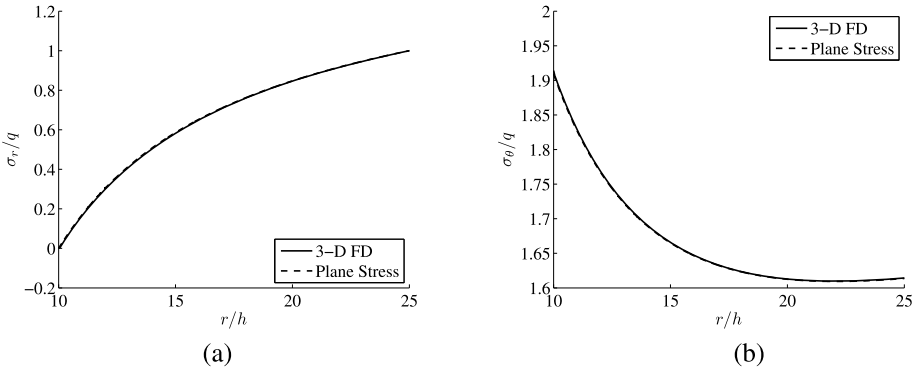


**Fig. 10** The variation of the (**a**) radial, and (**b**) circumferential stress under external pressure $q$ in the case $b = 2.5a = 25h$ and $m = 0.5$

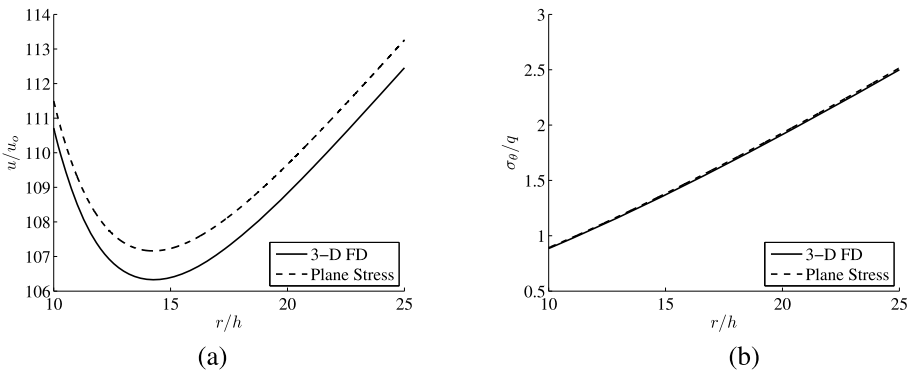


**Fig. 11** The variation of the (**a**) radial displacement, and (**b**) circumferential stress under external pressure $q$ in the case $b = 2.5a = 25h$ and $m = 2$

$\sigma_z$ and $\sigma_{zr}$ remain orders of magnitude smaller than the applied stress $q$ and the maximum hoop stress.

The numerical study also reveals that for a fixed ratio $b/a$ and a fixed nonuniformity parameter $m$, the discrepancy between the three-dimensional and the plane stress calculations, as well as the magnitude of $\sigma_z$ and $\sigma_{zr}$ stresses, is smaller for the thinner disks (smaller $h/a$ ratio). The same trend is observed for disks with different ratio $b/a$ and different parameter $m$, but the same ratio $E(b)/E(a) = (b/a)^m$: the plane stress approximation is better for a disk with smaller ratio $h/(b-a)$. Figures 12 and 13 show the results for a thick disk with $b = 2.5a = 5h$ and $m = -2$. The adopted finite difference mesh was $360 \times 60$. The radial and circumferential stresses are observably non-constant across the height of the disk, although still only mildly different from the constant values predicted by the plane stress model (Fig. 13). The $r$-variation of the radial and circumferential stress is close to that predicted by the plane stress model. The finite difference solution yields the maximum shear stress $\sigma_{zr}^{\max} = 0.287q$ to be almost 30% of the applied stress $q$, but less than 6% of the maximum hoop stress $\sigma_\theta^{\max} = 4.986q$ (Fig. 12).

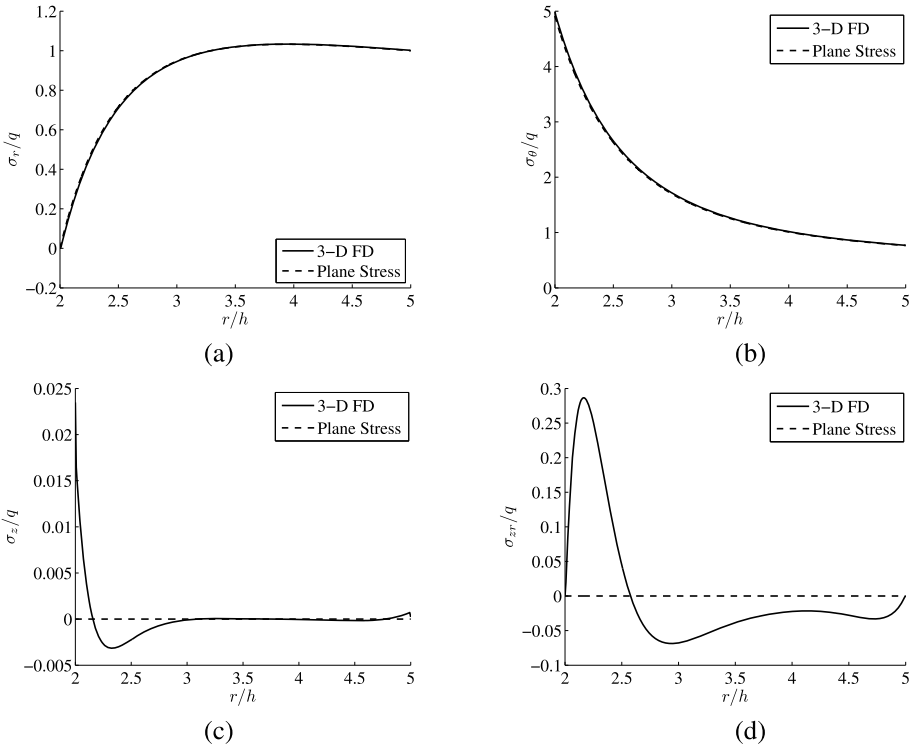


**Fig. 12** The variation of all four stress components along the horizontal section $z = h/4$ in a thick disk with $b = 2.5a = 5h$ and $m = -2$, due to external tension $q$

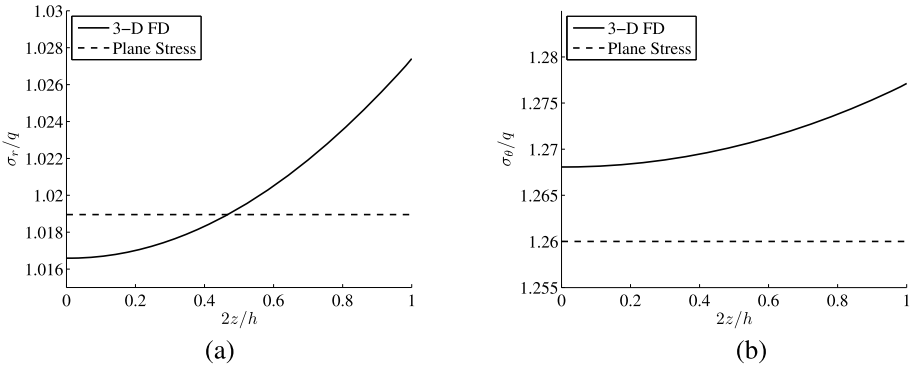


**Fig. 13** The variation of (**a**) radial, and (**b**) circumferential stress along the vertical section $r = (b - a)/2$ in a thick disk with $b = 2.5a = 5h$ and $m = -2$, due to external tension $q$

## A.2 Generalized Plane Stress

The average shear stress over the height of the disk vanishes ($\bar{\sigma}_{zr} = 0$), because $\sigma_{zr}(r, z)$ must be an odd function of $z$, by the symmetry considerations. Since $\sigma_z(r, z)$ must be an even function of $z$, the average normal stress $\bar{\sigma}_z$ does not vanish. Nonetheless, by taking the

averages in (A.7), the second equation is identically satisfied, while the first becomes

$$\frac{\partial \bar{\sigma}_r}{\partial r} + \frac{1}{r}(\bar{\sigma}_r - \bar{\sigma}_\theta) = 0. \tag{A.13}$$

Similarly, by taking the averages in (A.5), the first equation gives

$$r\frac{\partial \bar{\epsilon}_\theta}{\partial r} + \bar{\epsilon}_\theta - \bar{\epsilon}_r = 0, \tag{A.14}$$

where $\bar{\epsilon}_r = \partial \bar{u}/\partial r$ and $\bar{\epsilon}_\theta = \bar{u}/r$. It is noted that $u$ is an even, while $w$ is an odd function of $z$, so that $\bar{w} = 0$ and $\bar{\epsilon}_z = 2w(r, h/2)/h$. By integrating the second equation in (A.5) over the height $h$ of the disk, we obtain

$$r\int_{-h/2}^{h/2} \frac{\partial^2 \epsilon_\theta}{\partial z^2}\,\mathrm{d}z = \int_{-h/2}^{h/2} \frac{\partial^2 u}{\partial z^2}\,\mathrm{d}z = \left[\frac{\partial u(r,z)}{\partial z}\right]_{z=h/2} - \left[\frac{\partial u(r,z)}{\partial z}\right]_{z=-h/2}, \tag{A.15}$$

$$\frac{\partial}{\partial r}\int_{-h/2}^{h/2} \epsilon_z\,\mathrm{d}z = \frac{\partial}{\partial r}\int_{-h/2}^{h/2} \frac{\partial w}{\partial z}\,\mathrm{d}z = \frac{\partial w(r,h/2)}{\partial r} - \frac{\partial w(r,-h/2)}{\partial r}, \tag{A.16}$$

so that their sum is

$$r\int_{-h/2}^{h/2} \frac{\partial^2 \epsilon_\theta}{\partial z^2}\,\mathrm{d}z + \frac{\partial}{\partial r}\int_{-h/2}^{h/2} \epsilon_z\,\mathrm{d}z = 2\big[\epsilon_{zr}(r,h/2) - \epsilon_{zr}(r,-h/2)\big]. \tag{A.17}$$

The integration of the remaining term on the right-hand side of $(A.5)_2$ gives

$$-2\int_{-h/2}^{h/2} \frac{\partial \epsilon_{zr}}{\partial z}\,\mathrm{d}z = -2\big[\epsilon_{zr}(r,h/2) - \epsilon_{zr}(r,-h/2)\big]. \tag{A.18}$$

The last two expressions add to zero. Therefore, although the compatibility condition $(A.5)_2$ is not satisfied locally, at every point $(r, z)$, the average of the incompatibility component $L_r$ over the height of the disk vanishes at every $r$, i.e.,

$$\bar{L}_r = \frac{1}{h}\int_{-h/2}^{h/2} L_r\,\mathrm{d}z = 0, \quad L_r = r\frac{\partial^2 \epsilon_\theta}{\partial z^2} + \frac{\partial \epsilon_z}{\partial r} - 2\frac{\partial \epsilon_{zr}}{\partial z}, \tag{A.19}$$

supporting the plane stress modeling of sufficiently thin disks.

## Appendix B: Generalized Plane Strain

A long pressurized hollow cylinder is considered with the longitudinal stress $\sigma_z$ at two ends adjusted so that $\epsilon_z = \epsilon_z^0 = \text{const.} \neq 0$, giving rise to longitudinal displacement $w = \epsilon_z^0 z$. The radial component of displacement depends on the radial distance only, $u = u(r)$, and by symmetry $v = 0$. These assumptions lead to the exact solution, with the stress components $\sigma_r$, $\sigma_\theta$, and $\sigma_z$ dependent on $r$ only, while the other stress components vanish ($\sigma_{zr} = \sigma_{r\theta} = \sigma_{\theta z}$). In the case of a cylindrically anisotropic but uniform material, the solution can be found in [30] and [3].

The stress-strain relations of the orthotropic, radially nonuniform generalized plane strain problem are

$$\begin{aligned}\epsilon_r &= \frac{1}{E_\theta}(\alpha\sigma_r - \beta\sigma_\theta) - \nu_{zr}\epsilon_z^0,\\ \epsilon_\theta &= \frac{1}{E_\theta}(\gamma\sigma_\theta - \beta\sigma_r) - \nu_{z\theta}\epsilon_z^0,\end{aligned} \tag{B.1}$$

where $\epsilon_r = \mathrm{d}u/\mathrm{d}r$ and $\epsilon_\theta = u/r$. The longitudinal stress is

$$\sigma_z = E_z\epsilon_z^0 + \nu_{zr}\sigma_r + \nu_{z\theta}\sigma_\theta. \tag{B.2}$$

The inverted form of (B.1) is

$$\begin{aligned}\sigma_r &= \frac{E_\theta}{\alpha\gamma - \beta^2}\big[\gamma\epsilon_r + \beta\epsilon_\theta + (\gamma\nu_{zr} + \beta\nu_{z\theta})\epsilon_z^0\big],\\ \sigma_\theta &= \frac{E_\theta}{\alpha\gamma - \beta^2}\big[\beta\epsilon_r + \alpha\epsilon_\theta + (\beta\nu_{zr} + \alpha\nu_{z\theta})\epsilon_z^0\big].\end{aligned} \tag{B.3}$$

The equilibrium equation and the Saint-Venant compatibility condition are

$$\frac{\mathrm{d}\sigma_r}{\mathrm{d}r} + \frac{\sigma_r - \sigma_\theta}{r} = 0, \qquad \frac{\mathrm{d}\epsilon_\theta}{\mathrm{d}r} + \frac{\epsilon_\theta - \epsilon_r}{r} = 0. \tag{B.4}$$

The corresponding Beltrami–Michell compatibility condition is

$$\frac{\mathrm{d}\sigma_\theta}{\mathrm{d}r} + \frac{1}{r}\big[(1-m)\sigma_\theta - \varphi\sigma_r\big] = \frac{\nu_{z\theta} - \nu_{zr}}{\gamma}E_\theta\frac{\epsilon_z^0}{r}, \tag{B.5}$$

where

$$\varphi = \frac{\alpha - m\beta}{\gamma} = \frac{k(1 - \nu_{rz}\nu_{zr}) - m(\nu_{\theta r} + \nu_{\theta z}\nu_{zr})}{1 - \nu_{\theta z}\nu_{z\theta}}. \tag{B.6}$$

Together, (B.4) with (B.5), give the differential equation for the radial stress,

$$r^2\frac{\mathrm{d}^2\sigma_r}{\mathrm{d}r^2} + (3-m)r\frac{\mathrm{d}\sigma_r}{\mathrm{d}r} + (1 - m - \varphi)\sigma_r = \frac{\nu_{z\theta} - \nu_{zr}}{\gamma}E_\theta\epsilon_z^0. \tag{B.7}$$

The general solution of this nonhomogeneous second-order differential equation is

$$\sigma_r = Ar^{-n_1} + Br^{-n_2} + \eta_0 E_\theta\epsilon_z^0, \quad \eta_0 = \frac{\nu_{z\theta} - \nu_{zr}}{\gamma(1 - m - \varphi)}, \tag{B.8}$$

where $A$ and $B$ are integration constants, and

$$n_{1,2} = \frac{1}{2}(2 - m \mp s), \quad s = \big(m^2 + 4\varphi\big)^{1/2}. \tag{B.9}$$

The accompanying circumferential stress is

$$\sigma_\theta = (1 - n_1)Ar^{-n_1} + (1 - n_2)Br^{-n_2} + \eta_0 E_\theta\epsilon_z^0. \tag{B.10}$$

Having established the expression (B.8) and (B.10) for the radial and hoop stress, the longitudinal stress can be determined from (B.2). The result is

$$\sigma_z = G_0\epsilon_z^0 + g_1 A r^{-n_1} + g_2 B r^{-n_2}, \tag{B.11}$$

where

$$g_1 = \nu_{zr} + \nu_{z\theta}(1-n_1), \qquad g_2 = \nu_{zr} + \nu_{z\theta}(1-n_2), \qquad G_0 = E_z + \eta_0 E_\theta(\nu_{zr} + \nu_{z\theta}). \tag{B.12}$$

Finally, the displacement is deduced from the circumferential strain as $u = r\epsilon_\theta$, where the hoop strain $\epsilon_\theta$ is determined from the second of (B.3), and the expressions (B.8) and (B.10). This gives

$$u = \frac{b}{E_\theta^b}\left(\frac{b}{r}\right)^{m-1}\left(\eta_1 A r^{-n_1} + \eta_2 B r^{-n_2}\right) + \left[(\gamma-\beta)\eta_0 - \nu_{z\theta}\right]\epsilon_z^0 r, \tag{B.13}$$

with the parameters $\eta_1 = \gamma(1-n_1) - \beta$ and $\eta_2 = \gamma(1-n_2) - \beta$.

The total force at the end of the cylinder (or any cross section $z = \text{const.}$) is calculated from

$$F_z = 2\pi \int_a^b \sigma_z r \, \mathrm{d}r, \tag{B.14}$$

which gives

$$F_z = \pi\left(b^2 - a^2\right)G_0\epsilon_z^0 + \frac{2\pi g_1 A}{2-n_1}\left(b^{2-n_1} - a^{2-n_1}\right) + \frac{2\pi g_2 B}{2-n_2}\left(b^{2-n_2} - a^{2-n_2}\right). \tag{B.15}$$

If it is required that this force is equal to zero, the longitudinal strain must be such that

$$G_0\epsilon_z^0 = -\frac{2}{b^2-a^2}\left[\frac{g_1 A}{2-n_1}\left(b^{2-n_1} - a^{2-n_1}\right) + \frac{g_2 B}{2-n_2}\left(b^{2-n_2} - a^{2-n_2}\right)\right]. \tag{B.16}$$

## Appendix C: Positive-definiteness of (5.3)

In this appendix we prove the positive-definiteness of the left-hand sides in (5.3). For a disk, the inequality to prove is

$$m^2 - 4m\nu_{\theta r} + 4k > 0, \tag{C.1}$$

subject to the condition that $|\nu_{\theta r}| < k^{1/2}$. If $m > 0$, it is sufficient to prove that (C.1) holds for $\nu_{\theta r} = k^{1/2}$. This is obviously the case, because

$$m^2 - 4mk^{1/2} + 4k = \left(m - 2k^{1/2}\right)^2 > 0. \tag{C.2}$$

If $m < 0$, it is sufficient to prove that (C.1) holds for $\nu_{\theta r} = -k^{1/2}$. This is so, because

$$m^2 + 4mk^{1/2} + 4k = \left(m + 2k^{1/2}\right)^2 > 0. \tag{C.3}$$

For a sphere, the inequality to prove is

$$(1+m)^2(1-\nu_{\phi\theta}) - 8(1+m)\nu_{\theta r} + 8k > 0, \tag{C.4}$$

subject to the conditions imposed by the positive-definiteness of the strain energy,

$$-k^{1/2} < \nu_{\theta r} < k^{1/2}, \qquad 1 - \nu_{\phi\theta} > 2\frac{\nu_{\theta r}^2}{k}. \tag{C.5}$$

In view of (C.5), it is sufficient to prove that (C.4) holds for $1 - \nu_{\phi\theta} = 2\nu_{\theta r}^2/k$. This is so, because in this case (C.4) can be recast as

$$\left[(1+m)\nu_{\theta r} - 2k\right]^2 > 0. \tag{C.6}$$

A general proof of the third inequality in (5.3), corresponding to a nonuniform cylindrically anisotropic cylinder,

$$m^2(1 - \nu_{\theta z}\nu_{z\theta}) - 4m(\nu_{\theta r} + \nu_{\theta z}\nu_{zr}) + 4k(1 - \nu_{rz}\nu_{zr}) > 0, \tag{C.7}$$

is more difficult, but the proves in three important special cases can be readily constructed. For a uniform anisotropic cylinder ($m = 0$), the inequality (C.7) reduces to

$$4k(1 - \nu_{rz}\nu_{zr}) > 0, \tag{C.8}$$

which holds because $0 < \nu_{rz}\nu_{zr} < 1$. For a nonuniform ($m \neq 0$), but isotropic ($k = 1$) cylinder, the inequality (C.7) reduces to

$$m^2 - 4m\frac{\nu}{1-\nu} + 4 > 0, \tag{C.9}$$

subject to the condition

$$0 < \frac{\nu}{1-\nu} < 1, \tag{C.10}$$

because $0 < \nu < 1/2$. If $m > 0$, it is sufficient to prove that (C.9) holds for $\nu = 1$. This is the case because $(m-2)^2 > 0$. If $m < 0$, it is sufficient to prove that (C.9) holds for $\nu = 0$, which is the case because $m^2 + 4 > 0$.

Finally, if the cylinder is locally transversely isotropic, with the axis of local isotropy parallel to the $z$-axis, then $k = 1$, $\nu_{r\theta} = \nu_{\theta r}$, $\nu_{\theta z} = \nu_{rz}$, and $\nu_{z\theta} = \nu_{zr}$. The inequality to prove is then

$$m^2(1 - \nu_{\theta z}\nu_{z\theta}) - 4m(\nu_{\theta r} + \nu_{\theta z}\nu_{z\theta}) + 4k(1 - \nu_{\theta z}\nu_{z\theta}) > 0. \tag{C.11}$$

The positive-definiteness of the strain energy in this case requires that $-1 < \nu_{\theta r} < 1$, $0 < \nu_{\theta z}\nu_{z\theta} < 1$, and $(1 - \nu_{\theta r}) > 2\nu_{\theta z}\nu_{z\theta}$. The latest inequality can be rewritten in a more convenient form as

$$1 - \nu_{\theta z}\nu_{z\theta} > \nu_{\theta r} + \nu_{\theta z}\nu_{z\theta}. \tag{C.12}$$

If $m > 0$, it is sufficient to prove that (C.11) holds for $1 - \nu_{\theta z}\nu_{z\theta} = \nu_{\theta r} + \nu_{\theta z}\nu_{z\theta}$. This is the case, because (C.11) can then be recast as

$$(1 - \nu_{\theta z}\nu_{z\theta})(m-2)^2 > 0, \tag{C.13}$$

which is positive because $\nu_{\theta z}\nu_{z\theta} < 1$. If $m < 0$, (C.11) holds because it can be rewritten as

$$(1 - \nu_{\theta z}\nu_{z\theta})(m-2)^2 - 4m(1 + \nu_{\theta r}) > 0, \tag{C.14}$$

which is positive, because $\nu_{\theta r} > -1$ and $\nu_{\theta z}\nu_{z\theta} < 1$.

## References


1. Aguiar, A.R.: Local and global injective solution of the rotationally symmetric sphere problem. J. Elast. **84**, 99–129 (2006)
2. Aguiar, A., Fosdick, R.: Self-intersection in elasticity. Int. J. Solids Struct. **38**, 4797–4823 (2001)
3. Aguiar, A.R., Fosdick, R.L., Sánchez, J.A.G.: A study of penalty formulations used in the numerical approximation of a radially symmetric elasticity problem. J. Mech. Mater. Struct. **3**, 1403–1427 (2008)
4. Antman, S.S., Negrón-Marrero, P.V.: The remarkable nature of radially symmetric equilibrium states of aelotropic nonlinearly elastic bodies. J. Elast. **18**, 131–164 (1987)
5. Batra, R.C., Iaccarino, G.L.: Exact solutions for radial deformations of a functionally graded isotropic and incompressible second-order elastic cylinder. Int. J. Non-Linear Mech. **43**, 383–398 (2008)
6. Boresi, A.P., Chong, K.P.: Elasticity in Engineering Mechanics. Wiley, New York (2000)
7. Christensen, R.M.: Properties of carbon fibers. J. Mech. Phys. Solids **42**, 681–695 (1994)
8. Erdogan, E.: Fracture mechanics of functionally graded materials. Compos. Eng. **5**, 753–770 (1995)
9. Fosdick, R.L., Royer-Carfagni, G.: The constraint of local injectivity in linear elasticity theory. Proc. R. Soc. Lond. A **457**, 2167–2187 (2001)
10. Fosdick, R.L., Freddi, F., Royer-Carfagni, G.: Bifurcation instability in linear elasticity with the constraint of local injectivity. J. Elast. **90**, 99–126 (2008)
11. Freddi, F., Royer-Carfagni, G.: From non-linear elasticity to linearized theory: examples defying intuition. J. Elast. **96**, 1–26 (2009)
12. Froli, M.: Distribuzione ottimalle dei moduli elastici in corone circolari non omogenee. Atti Ist. Sci. Costr. Univ. Pisa **18**(251), 13–25 (1987)
13. Galmudi, D., Dvorkin, J.: Stresses in anisotropic cylinders. Mech. Res. Commun. **22**, 109–113 (1995)
14. Giannakopoulos, A.E., Suresh, S., Finot, M., Ollson, M.: Elastoplastic analysis of thermal cycling: layered materials with compositional gradient. Acta Metall. Mater. **43**, 1335–1354 (1995)
15. Green, D.W., Winandy, J.E., Kretschmann, D.E.: Mechanical properties of wood. In: Wood Handbook—Wood as an Engineering Material (Centennial edition), pp. 4-1–4-45. Forest Products Laboratory, United States Department of Agriculture Forest Service, Madison (2010)
16. Horgan, C.O., Baxter, S.C.: Effects of curvilinear anisotropy on radially symmetric stresses in anisotropic linearly elastic solids. J. Elast. **42**, 31–48 (1996)
17. Horgan, C.O., Chan, A.M.: The pressurized hollow cylinder or disk problem for functionally graded isotropic linearly elastic materials. J. Elast. **55**, 43–59 (1999)
18. Horgan, C.O., Chan, A.M.: The stress response of functionally graded isotropic linearly elastic rotating disks. J. Elast. **55**, 219–230 (1999)
19. Jin, Z.-H., Batra, R.C.: Some basic fracture mechanics concepts in functionally graded materials. J. Mech. Phys. Solids **44**, 1221–1235 (1996)
20. Kirchner, H.O.K.: Elastically anisotropic angularly inhomogeneous media. I. A new formalism. Philos. Mag., B **60**, 423–432 (1989)
21. Lekhnitskii, S.G.: Theory of Elasticity of an Anisotropic Body. Mir, Moscow (1981)
22. Lekhnitskii, S.G.: Anisotropic Plates, 2nd edn. Gordon & Breach, New York (1987)
23. Lubarda, V.A.: Remarks on axially and centrally symmetric elasticity problems. Int. J. Eng. Sci. **47**, 642–647 (2009)
24. Lubarda, V.A.: Elastic response of radially nonuniform, curvilinearly anisotropic solid and hollow disks, cylinders and spheres. Proc. Monten. Acad. Sci. Arts **20** (2012, to appear)
25. Roy, S.C.: Radial deformation of a nonhomogeneous spherically isotropic elastic sphere with a concentric spherical inclusion. Proc. Indian Acad. Sci., Sect. A, Phys. Sci. **85 A**, 338–350 (1977)
26. Shaffer, B.W.: Orthotropic annular disks in plane stress. J. Appl. Mech. **34**, 1027–1029 (1967)
27. Tarn, J.-Q.: Stress singularity in an elastic cylinder of cylindrically anisotropic materials. J. Elast. **69**, 1–13 (2002)
28. Theokaris, P.S., Philippidis, T.P.: True bounds on Poisson's ratios for transversely isotropic solids. J. Strain Anal. Eng. Des. **27**, 43–44 (1992)
29. Timoshenko, S.P., Goodier, J.N.: Theory of Elasticity, 3rd edn. McGraw-Hill, New York (1970)
30. Ting, T.C.T.: Pressuring, shearing, torsion and extension of a circular tube or bar of cylindrically anisotropic material. Proc. R. Soc. Lond. A **452**, 2397–2421 (1996)
31. Ting, T.C.T.: The remarkable nature of radially symmetric deformation of spherically uniform linear anisotropic elastic material. J. Elast. **53**, 47–64 (1999)
32. Ting, T.C.T.: New solutions to pressuring, shearing, torsion and extension of a cylindrically anisotropic elastic circular tube or bar. Proc. R. Soc. Lond. A **455**, 3527–3542 (1999)
33. Ting, T.C.T.: Poisson's ratio for anisotropic materials can have no bounds. Q. J. Mech. Appl. Math. **58**, 73–82 (2005)
34. Tutanku, N.: Stresses in thick-walled FGM cylinders with exponentially-varying properties. Eng. Struct. **29**, 2032–2035 (2007)
35. Ugural, A.C.: Stresses in Beams, Plates, and Shells, 3rd edn. CRC Press, Boca Raton (2009)